DEPARTMENT OF MANAGEMENT AND ENGINEERING

Factors Affecting the Finite Element Simulation of a ROPS Test of a Volvo Cab

Master Thesis carried out for Volvo CE AB
at the Division of Solid Mechanics
Linköping University
January 2007

Rikard Svärd

LIU-IEI-TEK-A--07/0014--SE

Linköping University
INSTITUTE OF TECHNOLOGY

Institute of Technology, Department of Management and Engineering
SE-581 83 Linköping, Sweden

Avdelning, institution
Division, Department

Div of Solid Mechanics
Dept of Management and Engineering
SE-581 83 LINKÖPING

Datum
Date

2007-01-15

Språk
Language

Svenska/Swedish
X Engelska/English

Rapporttyp
Report category

Licentiatavhandling
X Examensarbete
C-uppsats
D-uppsats
Övrig rapport

ISBN

ISRN

Serietitel och serienummer
Title of series, numbering

LIU-IEI-TEK-A--07/0014--SE

Titel
Title

Factors Affecting the Finite Element Simulation of a ROPS Test of a Volvo Cab

Författare
Author

Rikard Svärd

Sammanfattning
Abstract

The ability to protect the operator if a rollover of a construction equipment vehicle should take place is an essential requirement. In order to fulfil the necessities of this aspect, each cab constructed today is provided with a Rollover Protective Structure (ROPS).

The cabs developed by Volvo Construction Equipment undergo a ROPS-test. These tests are performed to ensure that the cab is able to uphold certain forces and consume certain energy levels without exceeding the restrictions in terms of displacements. As a part of the design process, Volvo uses simulations of these tests.

Comparisons made between tests and simulations have usually shown good agreements. This was not the case in a recent comparison of results. The objective of this thesis is to explain why the simulation of this test did not show satisfying agreement with the physical test.

By designing and constructing a welded component of standard beams and testing this as well as developing a finite element model of the component, an investigation of the influence of different parameters has been done.

The results from this thesis show that the major part of the divergence is due to non-correct material data. From yield tests and hardness measurements, material data has been obtained. These data show that the forming process, while manufacturing structural parts as well as welding these, strengthens the material with respect to the yield strength. Another major influence on the results comes from the modelling of welds in the FE-model.

With corrections for material data made in combination with a number of other changes of the model, results far better than the original are obtained.

Nyckelord: finite element, simulation, material data, welding, ROPS test
Keyword

Abstract

The ability to protect the operator if a rollover of a construction equipment vehicle should take place is an essential requirement. In order to fulfil the necessities of this aspect, each cab constructed today is provided with a Rollover Protective Structure (ROPS).

The cabs developed by Volvo Construction Equipment undergo a ROPS-test. These tests are performed to ensure that the cab is able to uphold certain forces and consume certain energy levels without exceeding the restrictions in terms of displacements. As a part of the design process, Volvo uses simulations of these tests.

Comparisons made between tests and simulations have usually shown good agreements. This was not the case in a recent comparison of results. The objective of this thesis is to explain why the simulation of this test did not show satisfying agreement with the physical test.

By designing and constructing a welded component of standard beams and testing this as well as developing a finite element model of the component, an investigation of the influence of different parameters has been done.

The results from this thesis show that the major part of the divergence is due to non-correct material data. From yield tests and hardness measurements, material data has been obtained. These data show that the forming process, while manufacturing structural parts as well as welding these, strengthens the material with respect to the yield strength. Another major influence on the results comes from the modelling of welds in the FE-model.

With corrections for material data made in combination with a number of other changes of the model, results far better than the original are obtained.

Sammanfattning

Förmågan att skydda föraren om en entreprenadmaskin välter är ett grundläggande krav på fordonet. För att säkerställa uppfyllandet av detta förses hytten med en skyddande struktur, en så kallad *Rollover Protective Structure* (ROPS).

De hytter som utvecklas och tillverkas av Volvo Construction Equipment genomgår prov av denna struktur. Proverna genomförs för att säkerställa att respektive hyttkonstruktion klarar vissa kraft- och energikrav utan att inträngningen av någon del blir för stor i hytten. Som en del i utvecklingsarbetet genomförs finita elementsimuleringar av dessa prover.

Prov – och beräkningsresultat har generellt uppvisat god överensstämmelse. Bakgrunden till detta examensarbete är ett fall där avvikelserna var tämligen stora.

En struktur konstruerad av balkar av samma slag som används i hytten har provats och detta prov har simulerats för att göra en studie av ingående finita elementparametrar. Materialdata har tagits fram med hjälp av drag- samt hårdhetsprov.

Arbetet visar att felaktiga materialdata var en stor anledning till avvikelserna. Fler faktorer, bland annat på vilket sätt svetsar modelleras, har en stor inverkan på resultatet.

Med korrigeringar gjorda för materialdata och ett antal andra faktorer erhålls resultat som är avsevärt bättre än de ursprungliga.

Preface

This thesis is the final assignment for graduation as a Master of Science in Mechanical Engineering. The work has been performed at the Division of Solid Mechanics, University of Linköping. It has been carried out for Volvo Construction Equipment with Engineering Research as a second company with interest of the work.

I would like to thank Anders Lindkvist, M.Sc. at Volvo, Prof. Larsgunnar Nilsson at the University of Linköping and Dr. Rikard Borg at ERAB for their help and guidance throughout the work. I would also like to thank Mr Ulf Bengtsson, Mrs Annette Billenius and Mr Bo Skoog at the University of Linköping for their help and support with test preparations and performances.

Linköping, January 2007
Rikard Svärd

Contents

1 Introduction

1.1 Background

Volvo Construction Equipment Cabs AB is located in Hallsberg. The company develop and manufacture cabs for construction equipment vehicles. For a cab to be approved for the use in a vehicle, a number of requirements have to be fulfilled. One of these is that the cab has to provide the operator with proper protection in the case of a vehicle turnover (rollover). The part of the cab structure that provides this protection is denoted as the Rollover Protective Structure (ROPS). Each type of cab has to be tested according to a standard that has been established by the industry. The test is not an actual rollover but sequential quasi-static tests in a controlled manner.

These tests are simulated with the Finite Element, FE, method to obtain results as basis for the development of the cabs. The simulations have in general shown good agreements with the corresponding tests. In this case however, the simulation showed results that did not agree with the corresponding test. The tests studied have been performed by Svensk Maskinprovning AB in Malmö and the simulations were performed by Engineering Research Nordic AB in Linköping.

1.2 Objective

The main objective of this thesis is to explain the divergent results between the tests and the simulations performed on a ROPS. A second objective has been to exclude as many parameters as possible from the potential reasons to erroneous results. As this means a study of different parameters, the thesis aims at concluding the influence of different parameters.

1.3 Procedure

The work has been divided into three main tasks. The first is to examine the models from the simulations and the tests performed in order to find possible reasons of divergence between the results. This has been done by comparing the geometry of the original CAD-data with the simulation model and test geometry, a study of boundary conditions and similar factors.

The other main task has been to create a simplified, welded structure made of standard beams used in the cab. This component has been modelled in the same way as the cab model and 5 test objects have been manufactured and tested. The model has been used to determine how different parameters in the FE-model influence the results.

The third task has been to test the material used in the cab structure with respect to its plastic behaviour. Further, a number of tests of the material properties have been performed to estimate the size and influence of the heat affected zones at the vicinity of the welds. The corners of the beam have been another aspect; they are plastically formed and therefore they probably have an increased yield strength. A series of tests has been performed to estimate this influence as well.

2 ROPS Test

2.1 Definitions

ROPS (rollover protective structures)
A system of structural members whose primary purpose is to provide a seated operator with reasonable protection in the event of a machine turnover (rollover). Non load-carrying members as doors and windows are excluded.

DLV (deflection-limiting volume)
A volume in the cab defined by an orthogonal approximation of a large, seated operator. No parts of the cab may penetrate this volume during the test. The size and placement are defined in a standard description; ISO 3164:1995.

LAP (load application point)
Point on the ROPS where the test load force is applied. LAP is also the point where the displacements are measured.

2.2 Test Procedure

To ensure that a cab manages to protect the driver in the event of a machine rollover, tests established by the International Standards Organisation (ISO) are carried out. The standard (ISO 3471) defines the loading of the cab as a quasi-static sequence performed with one or more hydraulic cylinder(s). The sequence consists of three parts; a lateral followed by a vertical and finally a longitudinal loading. In each case, the size of the required force depends on the machine weight and no part of the structure may intrude the DLV. When loading the ROPS in lateral direction a certain energy level has to be reached. This amount depends on the machine mass. The rate of deflection at the load application point shall not exceed 5 mm/s. Further, the systems used to measure mass, force and deflection shall be capable of meeting the requirements of another standard, ISO 9248, except that force and deflection measurement capability shall be within + or – 5% of maximum values.

2.2.1 Lateral loading

A load distributor is used to avoid localized penetration of the ROPS structural members. The load distributor is basically a plate and may distribute the force over a length of maximum 80% of the ROPS length. The side loaded shall be that which gives the most severe deflections. The initial direction of the loading shall be horizontal and perpendicular to a vertical plane through the machine longitudinal centreline. During the loading, deformations may cause the direction of loading to change, which is permissible. The position of the LAP is defined on the basis of the DLV location. The loading shall continue until the force and energy levels have been reached. The energy is calculated as the area under the force-displacement curve obtained at the cylinder(s).

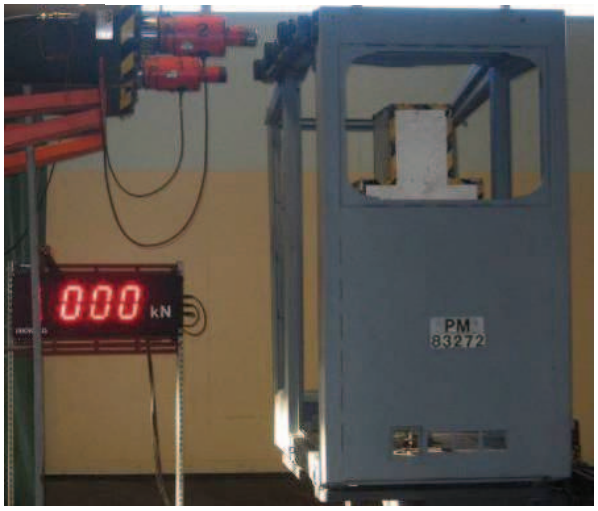

Figure 2.1. ROPS prior to lateral loading

2.2.2 Vertical loading

A load distributor is used in the vertical loading as well. The centre of the vertical load shall be applied in the same vertical plane, perpendicular to the longitudinal centreline of the ROPS, as the lateral load. The structure is loaded until the force level specified is reached and shall support this load for 5 minutes or until any deformation has ceased, whichever is shorter.

2.2.3 Longitudinal loading

After the vertical loading, a longitudinal load shall be applied to the ROPS. This load shall be applied along the longitudinal centreline of the ROPS, at a load point defined by the intersecting planes of the front and top surfaces. A load distributor may distribute the load over a length no greater than 80% of the width. The loading is to continue until the force level specified has been reached.

2.3 Test Results

The results from tests previously performed are presented in Figure 2.1.

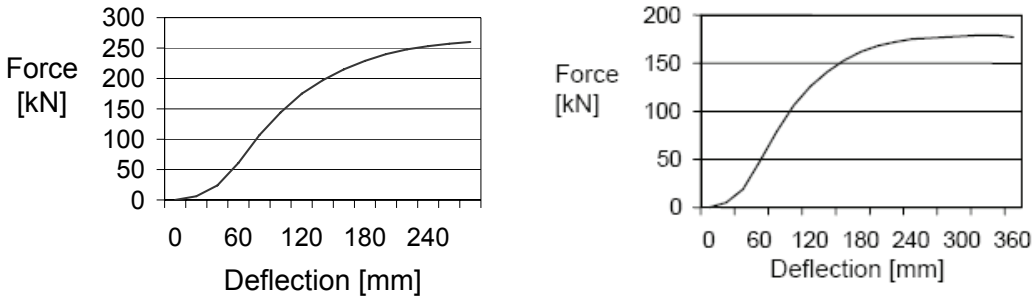

Figure 2.1. Lateral test results to the left and longitudinal test results to the right

3 FE Simulation of ROPS Test

3.1 FE Model

The FE simulations of the ROPS test have been performed by Engineering Research. This section describes how the cab is modelled and how the simulation is performed.

3.1.1 Geometry

The geometry of the test model is taken from the original CAD data from Volvo CE. That is, every part and its location are given from the same information as the drawings designed for manufacturing.

3.1.2 Boundary Conditions

The ends of the circular beam that the cab rests on are constrained from all translational and rotational movement.

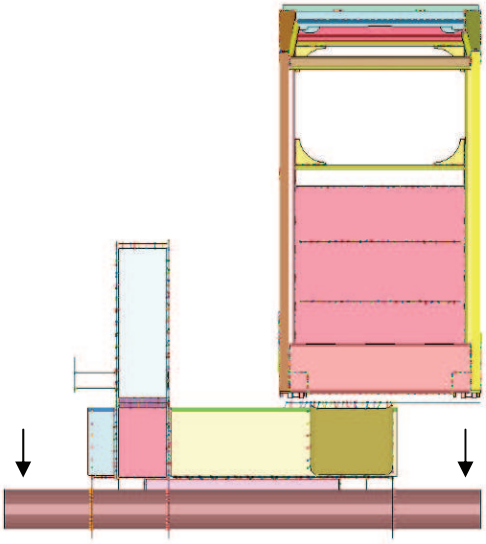

Figure 3.1. The ends of the circular beam (at the arrows) are constrained from translational and rotational movement

The load is applied by a load distributor given a prescribed motion. The load distributor is modelled as a rigid body with the displacements perpendicular to the loading direction constrained as well as rotations around the x-axis, see Figure 3.2. As in the testing, the loading is defined as prescribed displacements.

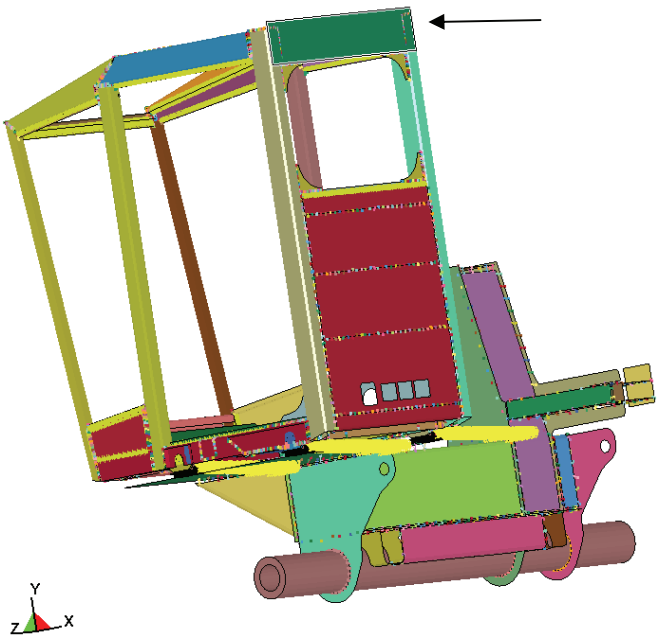

Figure 3.2. The cab model with the load distributor pointed out

3.1.3 Elements

The cab is modelled mainly with four-noded shell elements of an approximate size of 10x10 mm. The element type is the fully integrated shell element type 16 in LS-DYNA.

3.1.4 Material Models

The actual ROPS materials are modelled with a piecewise linear plasticity model. That is, the material deforms elastically using a Young's modulus up to the yield strength. Thereafter, the material deforms plastically according to a piecewise linear relation between the true stress and the true plastic strain in the plastic region.

The load distributor is modelled as a rigid body.

Some of the welds in the cab are modelled with a special material model defined specifically for welds. This is described in the next section.

3.1.5 Weld Modelling

For the long, straight parts welded together, an automatic type of weld model may be defined in LS-DYNA. This gives the possibilities to define a Young's moduli, Poisson's ratio and a plastic behavior of the weld material as well as the possibility to use failure criteria on the welds. By experience, failure in these tests is rare, why no

failure criterion has been used. The Young's moduli as well as Poisson's ratios are the same as adjacent parts in the structure. The weld is created between nodes of each part welded, and the weld material is used to connect them. The plastic behaviour is ignored by defining a very high yield strength of the weld material.

In the more complex geometrical areas, *constrained nodal rigid bodies* are used. They are modelled by connecting a number of nodes in each part welded, forming a rigid body.

3.2 Original Simulation Results

The original simulation results are presented and compared to the test results in figure 3.3.

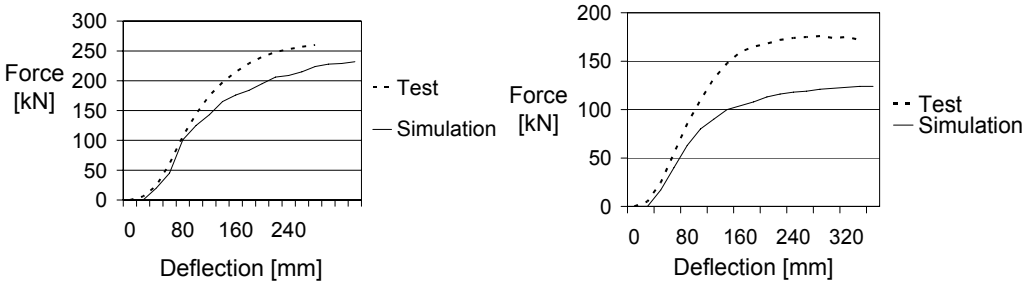

Figure 3.3. Lateral and longitudinal simulation and test results, respectively

4 Component

In order to evaluate different parameters and concepts of the simulation model, a sub component was developed, manufactured and tested. The test was also simulated in the finite element program LS-DYNA with different sets of design parameters.

4.1 Choice of Component

The idea has been to test a common structural component of the cab – two beams welded orthogonally to each other. The beams are standard thin-walled beams, with a square profile, also used as B-pillars in the cab. The original idea of geometry was a closed structure of four beams. Hand calculation showed that the test machine we had access to did not have the load capacity enough why the geometry in Figure 4.1 was proposed.

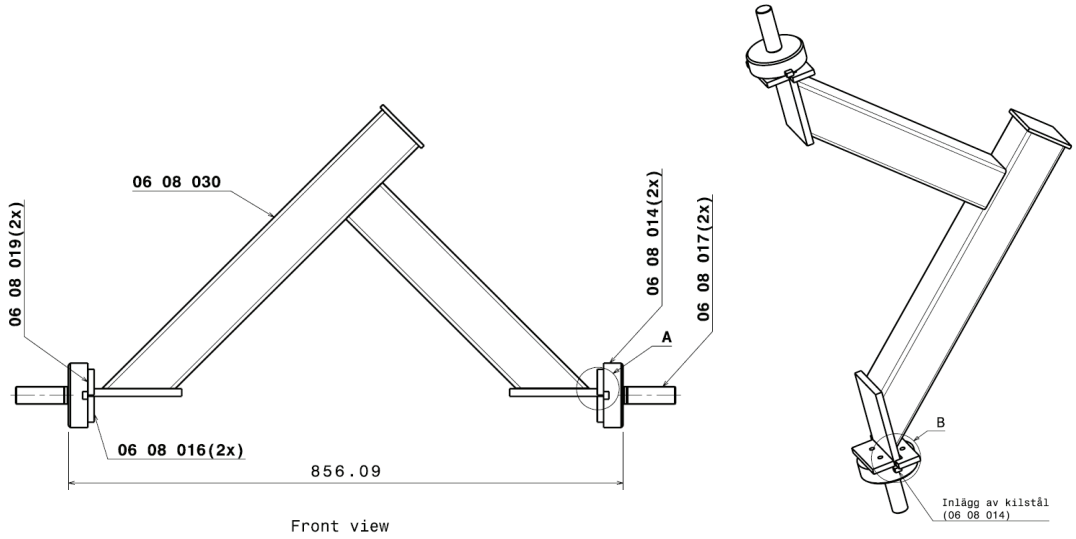

Figure 4.1. Component geometry

In order to verify that the test machine most probably would manage to plastically deform the structure, the following check was done.

Using the theorem of rigid plasticity and the upper bound theorem, a limit analysis may be done according to Odenö and Klarbring (1984). That is, an assumption is made that the cross section of a beam is fully plasticised when the moment acting on the beam corresponds to the stress in the entire cross section to be equal the yield limit of the material. When this moment is reached, the structure cannot carry any more load but will collapse.

In this case, the cross sections of the beams are quadratic with the width 80 mm and thickness 6 mm (the radius of the corners are neglected, i.e. in this case a conservative assumption).

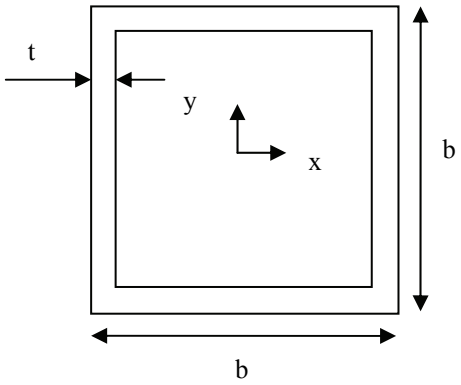

Figure 4.2. Simplified cross section of the beams

With side length *b* and thickness *t* according to Figure 4.2 the moment around the x-axis may be calculated using the yield limit σ_Y of the material

$$M_{fp}^{1} = 2\sigma_Y bt\frac{b}{2} \qquad (4.1a)$$

$$M_{fp}^{2} = 2\sigma_Y bt\frac{b}{4} \qquad (4.1b)$$

Where M_{fp}^{1} is the moment required to plasticise the lower and upper parts of the beam in Figure 4.2 and M_{fp}^{2} the moment required to plasticise the sides of the beam. The index $_{fp}$ means fully plastic.

M_{fp}^{1} and M_{fp}^{2} may now be added to a total moment M_{fp} needed to plasticise the entire cross section

$$M_{fp} = \frac{3b^2 t}{2}\sigma_Y \qquad (4.2)$$

The test object is to be loaded in compression in the horizontal direction according to the orientation of the left part of Figure 4.1. Referring to Odenö and Klarbring (1984), a collapse load calculated for an assumed collapse mechanism is equal to or greater than the true collapse load.

The assumption made here is that one plastic hinge is enough to collapse the structure according to Figure 4.3.

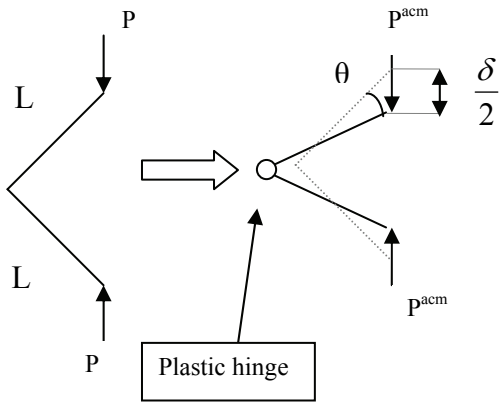

Figure 4.3. One plastic hinge at the joint is the assumed collapse mechanism (acm) which gives the change in angle θ for each beam and a total deflection δ. The beams have the length L and a force P is applied on the structure

The supplied power is equal to the dissipated power which gives the relation

$$P^{acm}\dot{\delta} = 2M_{fp}\,\dot{\theta} \qquad (4.3)$$

Where the dot above δ and θ indicates the time derivative of each variable. If δ is assumed small, the angle θ is also small and the simplification stated in Equation (4) may be done using the length L

$$\delta = L\sin\theta = L\theta \qquad (4.4)$$

The equations (2), (3) and (4) may now be combined to the following expression.

$$P^{acm} = \frac{2M_{fp}}{L} = \frac{3b^2t}{L}\sigma_Y \qquad (4.5)$$

The yield strength of the material is 355 MPa according to the material supplier. Due to the size of the test machine, the maximum allowable lengths of the beams are 452 mm on the inside of the component. By adding half the width of the beams, the length used for this calculation becomes 492 mm.

This gives numerically that the force needed according to the assumed collapse mechanism is

$$P^{acm} = \frac{3\cdot 80^2\cdot 6}{492}\cdot 355 = 83.1\,\text{kN} \qquad (4.6)$$

This is permissible since the maximum capacity of the test machine is approximately 100 kN.

The geometry was settled according to Figure 4.4 and the component was manufactured at Volvo CE.

Figure 4.4. One of the five test components

Drawings of the component are presented in Appendix A.

4.2 Test Procedure and Results

The tests were carried out at the University of Linköping in an INSTRON 5582 test machine. The test object was mounted in the machine as presented by Figure 4.5. The machine has a maximum force of 100 kN and the ability to deliver this force a distance corresponding to the length of the test objects. During the test performance the load cell included in the machine registered the force at the same time as the displacement was recorded. The software Bluehill was used to control the test and extract test results, which were defined as curves where the force is plotted as function of the displacement. The tests were carried out with a loading rate 5 mm/min, which certainly is to be considered as a static loading.

Figure 4.5. Component in test machine before loading

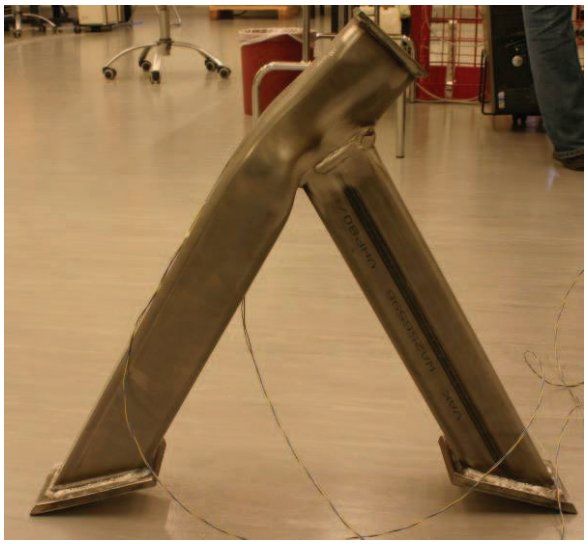

Figure 4.6. Component after test

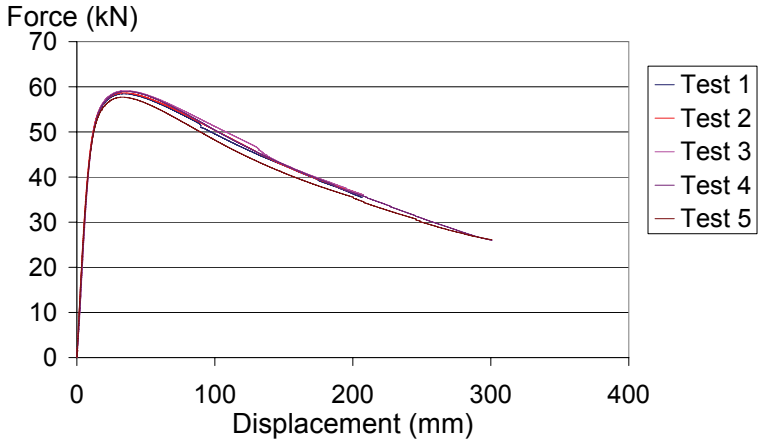

Figure 4.7. Test results of the component

As seen in Figure 4.7, the results from the component tests are homogeneous, with one small exception; test object 5 showed somewhat lower force level throughout the test. The first three tests were performed to a displacement of 200 mm and the last two tests to a displacement of 300 mm. Even though the results are more or less the same for the five tests, they are not totally identical. Test 2 is established as a representative result, why this is the case chosen for comparisons with the FE results in the following.

5 Material Testing

Correct material data is of great importance while striving for correct FE simulation results. The nominal yield strength of the material according to the supplier is greater than 355 MPa. Because of the uncertain mechanical properties of the beams used in the cab and the tested component, various mechanical tests have been made. The test procedures and results are presented in this section.

5.1 Tensile Test

5.1.1 Test Theory and Procedure

When a tensile test is performed, the measured quantities are the loading force and the displacement. The displacement is primarily measured with an extensometer as the *current* length L of the test length. The initial length L_0 in this case was 50 mm. The machine used was an INSTRON 5582. This machine is an electromechanical test machine, which in this case was controlled by the software Bluehill. The load cell of the machine measures the force.

The yield tests have been performed as described in the Swedish Standards Institutes document SS-EN 10002-1 (2001). This standard describes in details the test parameters such as the geometry of the test specimens and the maximum strain rate during loading. The geometry in Figure 5.1 presents some rather peculiar dimensions. This is due to the directives in the standard used, which defines certain relations, such as a dependency between the cross sectional area and the initial length.

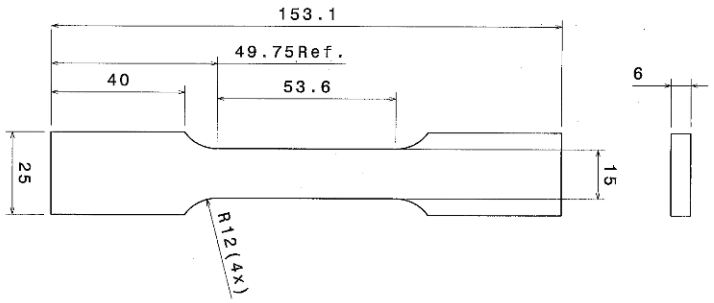

Figure 5.1. Geometry properties of the tensile test specimen

According to the standard, the speed of the test may not exceed 0.86 mm/min why a speed of 0.8 mm/min was used. Due to concerns of the test equipment, the yield tests were terminated at a strain of about 20%.

In order to evaluate the measured quantities and further on derive curves to use as input to LS-DYNA, the following expressions are useful.

The force F gives, divided by the original area Dahlberg (2001):

$$\sigma_E = \frac{F}{A_0} \tag{5.1}$$

Where σ_E is the engineering stress.

The *current* length L gives, together with the *initial* length L_0:

$$\varepsilon_E = \frac{L - L_0}{L_0} \tag{5.2}$$

Where ε_E is defined as the engineering strain.

The *true* stress σ_T may now be defined as

$$\sigma_T = \frac{F}{A} \tag{5.3}$$

where A is the *current* cross-section area of the test specimen.

The *true*, or logarithmic, strain ε_T for large deformations is Dahlberg (2001)

$$\varepsilon_T = \ln\left(\frac{L}{L_0}\right) \tag{5.4}$$

With the assumption that plastic deformation does not change the volume of the test specimen, the following expression may be used:

$$A_0 L_0 = AL \tag{5.5}$$

A reformulation of Equation (2) gives:

$$\frac{L}{L_0} = \varepsilon_E + 1 \tag{5.6}$$

Equation (6) in Equation (4) gives

$$\varepsilon_T = \ln(\varepsilon_E + 1) \tag{5.7}$$

Equation (1) and (3) may be combined to

$$\sigma_T = \frac{A_0}{A}\sigma_E \tag{5.8}$$

A combination of Equation (5) and (6) leads to

$$\frac{A_0}{A} = \frac{L}{L_0} = \varepsilon_E + 1 \qquad (5.9)$$

This may be used in Equation (8) to establish the expression

$$\sigma_T = \sigma_E(\varepsilon_E + 1) \qquad (5.10)$$

The equations above allow determination of the *true strain* and the *true stress* from the measured quantities and apply for strains below localization.

The engineering strain may be divided into one *elastic* part ε_E^{el} and one *plastic* part ε_E^{pl}, i.e.

$$\varepsilon_E = \varepsilon_E^{el} + \varepsilon_E^{pl} \qquad (5.11)$$

Using Equation (11) and the following expression Dahlberg (2001)

$$\varepsilon_E^{el} = \frac{\sigma_E}{E} \qquad (5.12)$$

where E is Young's modulus, give

$$\varepsilon_E^{pl} = \varepsilon_E - \frac{\sigma_E}{E} \qquad (5.13)$$

Equation (13) may finally be combined with Equation (7) as

$$\varepsilon_T^{pl} = \ln(\varepsilon_E - \frac{\sigma_E}{E} + 1) \qquad (5.14)$$

The results obtained from testing and calculated with Equations (10) and (14) will later be used as material data input in LS-DYNA.

5.1.2 Test Objects

The test objects are milled out from an extra component made for this purpose. All machining were performed with controlled cooling to minimise heat effects. The specimens are specified with respect to geometry in the previous section and further details are defined in the corresponding following sections.

None of the specimens were perfectly flat after being milled out. This implies the presence of rather large residual stresses. In total, seven test specimens were made and the extensometer was mounted on the convex and concave side every other time, respectively. No significant differences in the results were observed why no further notice was taken on this matter.

5.1.3 Nominal Test

The tests defined as *nominal* are milled out from the middle of a beam flange, Figure 5.3.

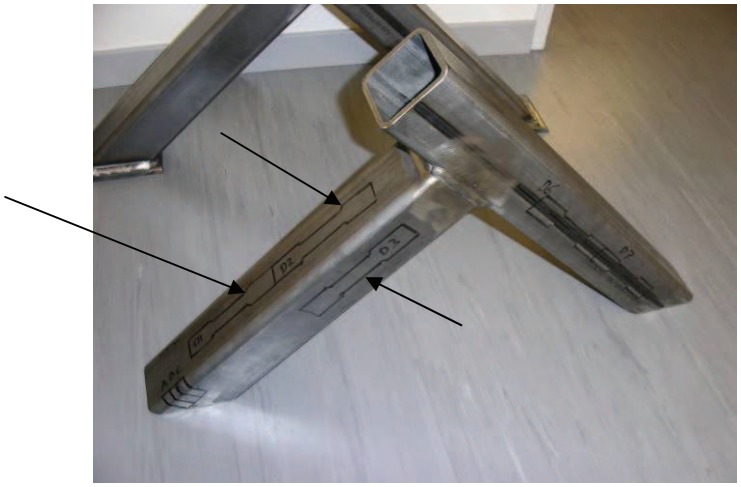

Figure 5.3. Test specimens before milled out of the beam

Figure 5.4. Test specimens D1 and D2. The upper D1 after testing and the lower D2 before testing

Five test specimens were milled out of the beams and tested. The test results are presented in Figure 5.5.

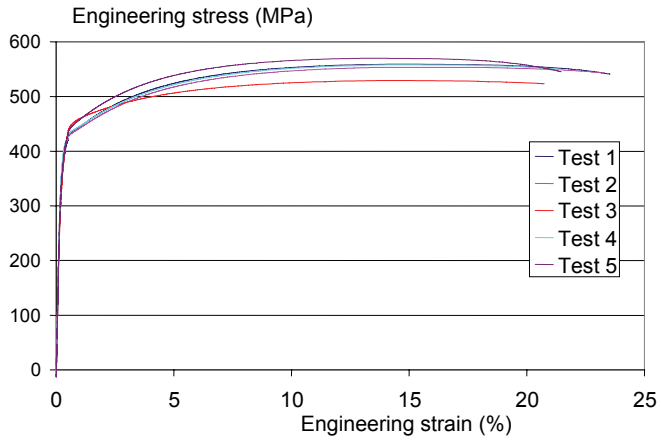

Figure 5.5. Nominal yield test results

The results from the specimens are quite equal, especially concerning the yield strength. The yield strength was found to be 415 MPa, significantly higher than the nominal 355 MPa guaranteed by the supplier.

5.1.4 Influence of Welding

The beam profiles are longitudinally welded along one of the flanges. In order to examine the influence of the longitudinal weld and later on study the relation between hardness and yield strength, two tests containing this weld were performed. The weld is completely flat on the outside of the beam but the weld material on the inside were milled away in order to grip the test specimens properly.

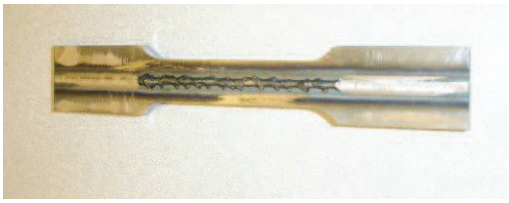

Figure 5.6. Test specimen containing a weld. The weld is milled at the wider areas at the end in order to grip the specimen properly

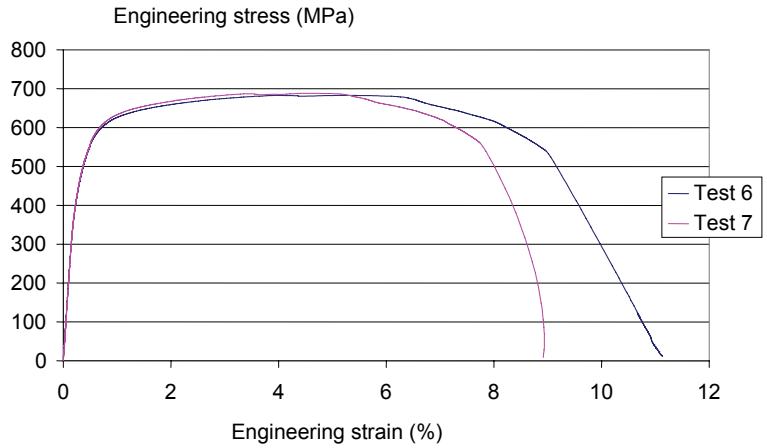

Figure 5.7. Tensile test results from the welded areas of a beam profile

The yield strength is approximately 50 % higher in the welded areas at the same time as the ductility is a lot lower. The welded area fracture at about 10 % strain while the nominal tests were stopped at about 20 % strain.

5.2 Hardness Test

5.2.1 Test Theory and Procedure

According to Davis et al. (1998) and the course file in Experimental Evaluation of Fatigue and Fracture, there are a linear relationship between the Vickers hardness and the yield strength of the kind of material used. The Vickers hardness of a material is measured by pressing a diamond into the test specimen. The diamond is a grinded pyramid with a top angel of 136˚, which gives two diagonals when pushed into the test specimen. The value of the Vickers hardness is then obtained from the mean value of these diagonals whose Vickers hardness Hv is derived according to

$$Hv = \frac{2F\sin(\frac{136^\circ}{2})}{d^2} \qquad (5.15)$$

where F is the test force in kp and 1 kp = 9,80665 N.
d is the mean of the diagonal length in mm.

Equation (15) may be simplified to

$$Hv = \frac{1{,}854F}{d^2} \qquad (5.16)$$

see Peng et al. (2005).

Before a test may be done, the test specimen has to be prepared by grinding. This is done to avoid rough surfaces which may give false results, e.g. due to the diamond hitting a top of the rough surface which would give a too small hardness value. The

preparation grinding is performed in 5 steps; by grinding with silicon papers of 220, 500, 1200, 2000 and 4000 grains per mm^2 respectively. For smaller objects (in this case the corners and the nominal test specimens) it is convenient to cast the specimen into a polymer material in order to fix and orient the test as desired before grinding.

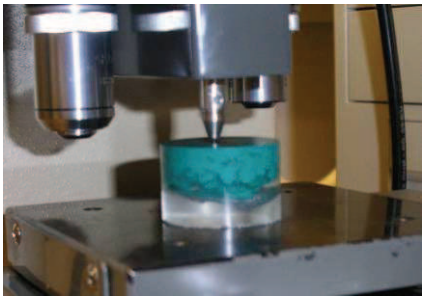

Figure 5.8. A test specimen in the hardness tester

The tests were carried out in a hardness tester called LECO M-400. This machine is basically a microscope with an indenter which may be loaded with a range of masses. The maximum mass 1 kg was chosen because of the higher accuracy that comes with a larger mass. The loading was held constant during 10 seconds before the diamond was removed. Next step was that the optical instrument was put in place to make a photo of the impression. The magnification used was 55x. The photo was then imported to the image analysis software called microGOP 2000/S. The four corners were marked on the screen, on which the program responds with a Vickers hardness value.

5.2.2 Test Objects

The aim of the hardness tests is to evaluate the changes in the material due to welding and the plastic deformation of the beams. The beams are roll formed and the data given by the material supplier is valid for plane sheets, i.e. not taking any cold forming into account. The test objects are therefore chosen as follows: In total five pieces for testing the welding and heat affected zones. Three pieces for testing the corners of a beam and three nominal test pieces picked in the middle of a beam.

The test objects for hardness measures were taken from the same component as the tension test objects and were milled out of the beams.

5.2.3 Nominal Test

To have a reference value for comparison of values from the heat affected zones and welds as well as the corners, a series of nominal tests were carried out. The three test objects showed uniform results from the test series carried out. In total, 18 measurements were performed and the result is presented in Table 5.1.

173,2	174,21	172,53	173,49	171,23	173,18
174,19	171,89	171,61	173,66	175,08	175,46
177,9	172,2	176,87	174,5	172,85	169,54

Table 5.1. Results from nominal hardness tests

The mean value was determined to be Hv=173,8 N/mm^2.

5.2.4 Influence of Welding

Two different kinds of welds are present in the structure. The first (1) is present in each beam; the beams are made from sheets that are roll formed to the desired shape and welded along the whole length. The other kind of weld (2) is the one that joins the beams together.

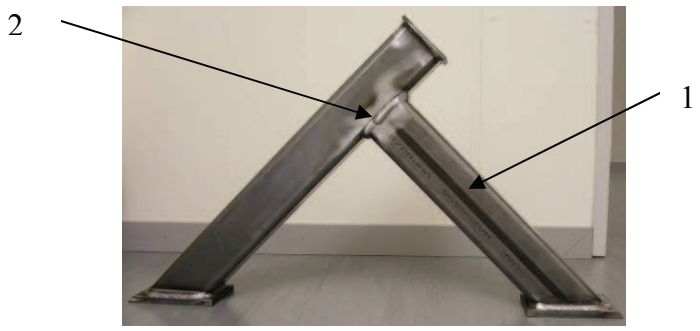

Figure 5.9. Two types of welds

The test specimens used were machined (milled) from the beams according to Figure 5.10.

The measurements of the first type of weld were made in the area corresponding to the tensile test specimens. Two test specimens were milled out of one of the beams and the hardness were measured across the pieces. The average of the two specimens were obtained as Hv = 231,5 N/mm^2 and Hv = 220,3 N/mm^2, respectively. This gives an average of both test specimens of Hv = 225,9 N/mm^2.

The linear relation between the Vickers hardness and the yield strength may now be verified. The yield strength of the test specimen milled out in the centre of the weld were determined to 537 MPa. The nominal test specimens gave a yield limit of 415 MPa which gives the quotient $\frac{537}{415}$ =1,29. The corresponding quotient of the Vickers hardness is $\frac{225,9}{173,8}$ = 1,30. That is, a linear relation between the Vickers hardness and yield limit of the material is verified. The linear relation is proposed by Davis et al. (1984) and Peng et al. (2005).

The second type of weld tested is the weld that joins the two beams together. The test specimens were milled out according to Figure 5.10.

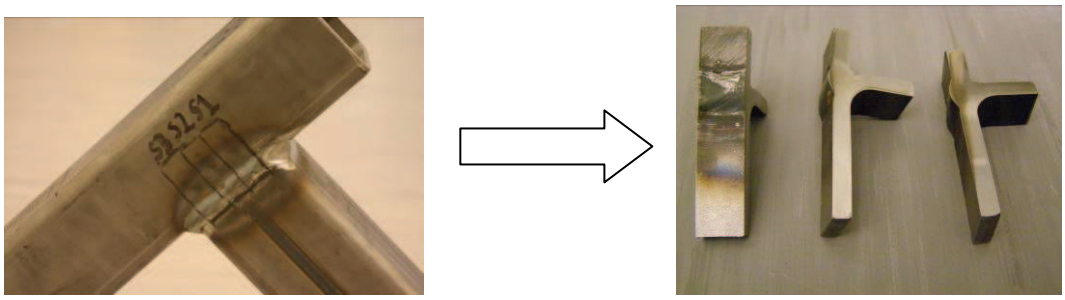

Figure 5.10. The locations of the test specimens and the grinded results

As presented in Figure 5.10, three test specimens were milled out and tested. The hardness measurements started in the middle of the weld and were then performed with a distance of 2 mm between each measurement along the specimen direction from the weld. The test results are presented in Figure 5.11.

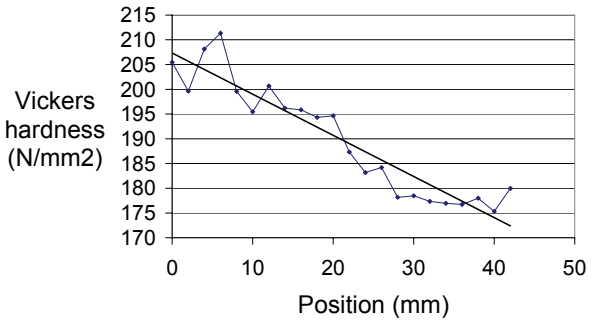

Figure 5.11. The Vickers hardness as function of distance from the centre of the weld. The dotted curve is a mean from three tests and the line a linearisation of the mean

5.2.5 Influence of the Forming Process

The material data provided by the material supplier is valid for a steel sheet before roll forming and welding. Due to the fact that the corners are plastically deformed, the material probably undergoes a change of behaviour. Therefore, tests have been performed to estimate this change.

The Vickers hardness were measured along the corners, Figure 5.11.

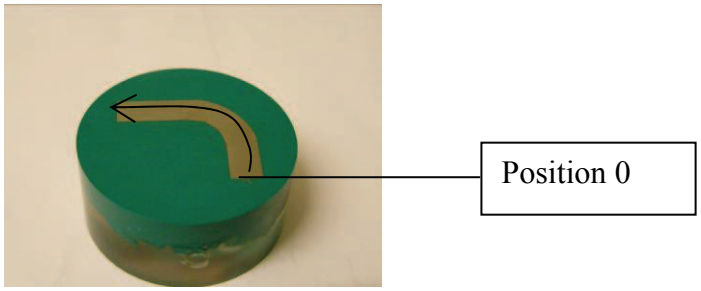

Figure 5.11. A corner test specimen in its polymer fixture. Position 0 defines the starting position of the measurements

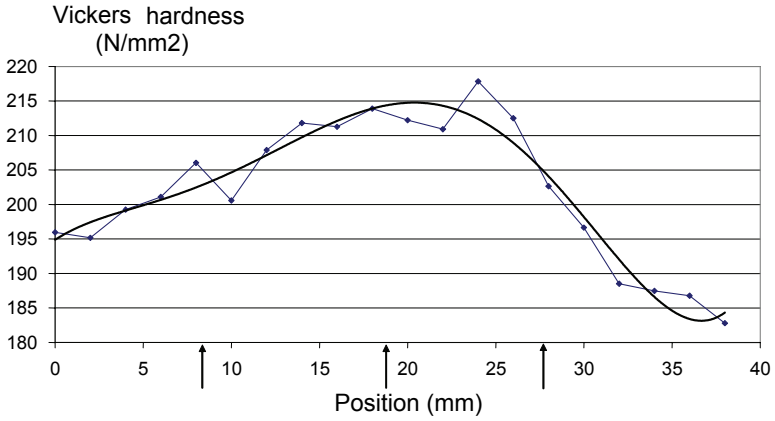

Figure 5.12. Vickers hardness as function of position. The start position is defined in Figure 5.11. The arrows points out the start, centre and end of the curvature at the corner, respectively. The dotted curve represents a mean value of the three test specimens and the smooth curve is a fifth order representation of the mean

By using the linear relation between Vickers hardness and yield strength combined with yield test data, the maximum yield strength in the corner is $415\frac{215}{174} = 513$ MPa.

6 FE Simulation of Component

6.1 FE Model

The geometric model for the simulations was created in the pre-processor TrueGrid, XYZ Scientific Applications, Inc (2001). That is, the different parts were modelled and divided into discrete elements in the latter software. The model was then transferred to the pre-and postprocessor LS-PrePost to complete the model with respect to material models, boundary conditions etc.

The basic model was made to be as comparable as possible to the cab model. The element size is similar, i.e. approximately 10x10 mm, the material parameters are similar, etc. A summation of the basic model follows.

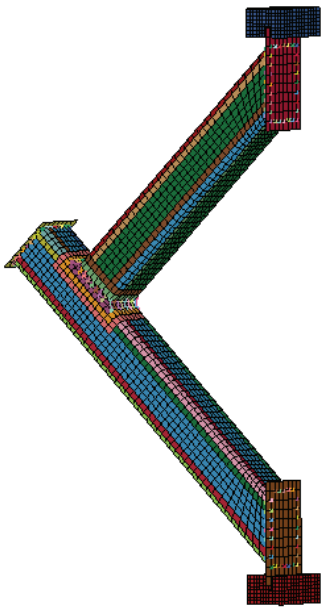

Figure 6.1. The basic model for FE simulations

The model includes the same parts as the tested component. In addition, two parts are added in order to define the boundary conditions. The lowermost part in Figure 6.1 is a rigid body which is constrained with respect to all translations and all rotations. A contact is defined between this part and the lower force plate of the actual component. The uppermost part is rigid also and all rotations are constrained. The difference from the lowermost part is the translation; the uppermost part is given a prescribed displacement downwards in Figure 6.1. In order to avoid peaks of reaction forces and dynamic responses, the curve defining the motion smoothes the displacement in the beginning of the loading, see Figure 6.2. Furthermore, this gives a better chance to correctly treat the contacts.

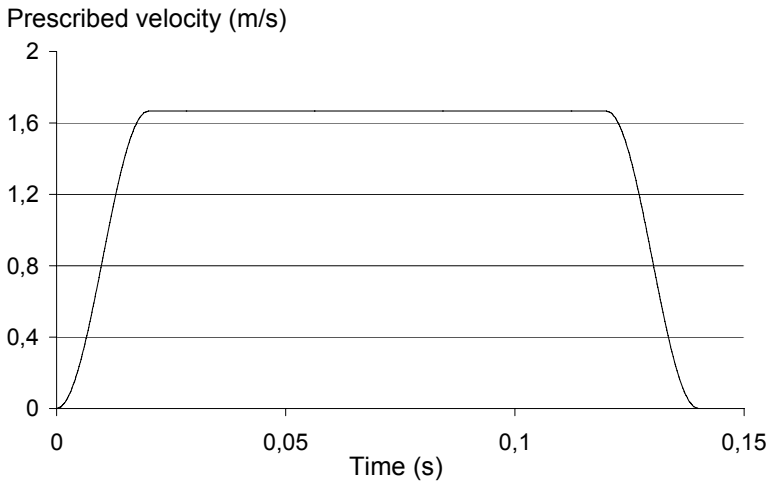

Figure 6.2. The prescribed displacement of the uppermost part in the FE model

The velocity of the uppermost part is high compared to the velocity used for testing the component. The high velocity is chosen to save computing time and could involve dynamic influences on the results. In order to check this, the level of kinetic energy is compared to the total energy throughout a simulation, Figure 6.3.

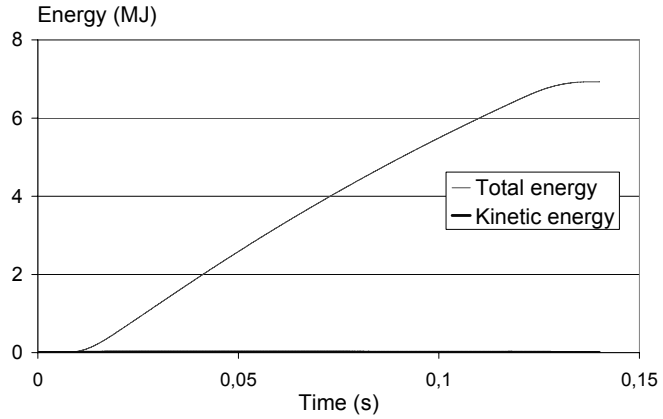

Figure 6.3. Total and kinetic energy vs. time. The kinetic energy is close to zero

The responses of the simulations do include oscillations. The response has been filtered in all result diagrams with an SAE filter at the threshold frequency 60 Hz.

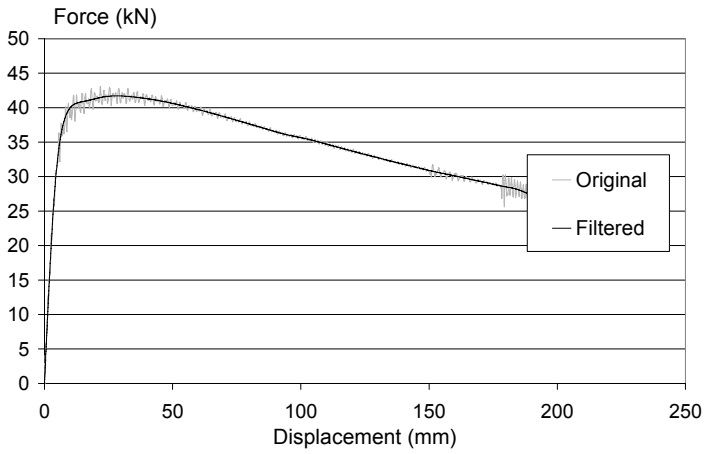

Figure 6.4 The effect of filtering, results from the basic model

The component is built up by five parts; two beams and three metal sheet parts. The parts are welded together and in the basic model this is modelled with constrained nodal rigid bodies (CNRB`s). The most of these connections are defined by one node in each of the two parts joined by the weld and represents a rigid body that connects them.

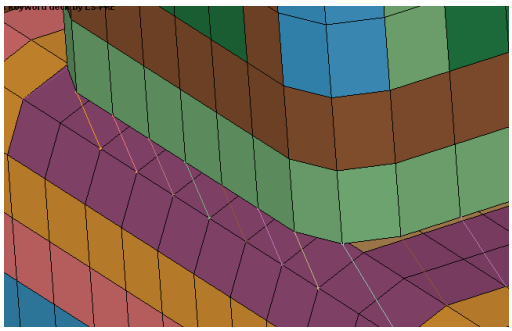

Figure 6.5. Example of nodal rigid bodies

The deformations of the FE model were in all models very much like the deformations in the tested component, Figure 6.6.

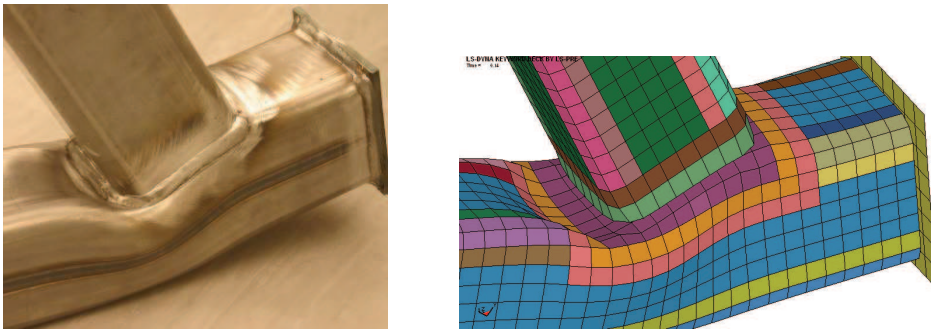

Figure 6.6. The deformed component to the left and the corresponding deformed FE model to the right

6.2 Investigation of Parameters

6.2.1 Number of elements

Two different models have been examined with respect to the number of elements, or element size. The first size was the same as in the cab model; approximately 10x10 mm. This gave a total of 3184 shell elements, which are used to model the component. The second size meant that each element length where divided into two, giving an element size 1/4 of the original and a total of 12736 shell elements.

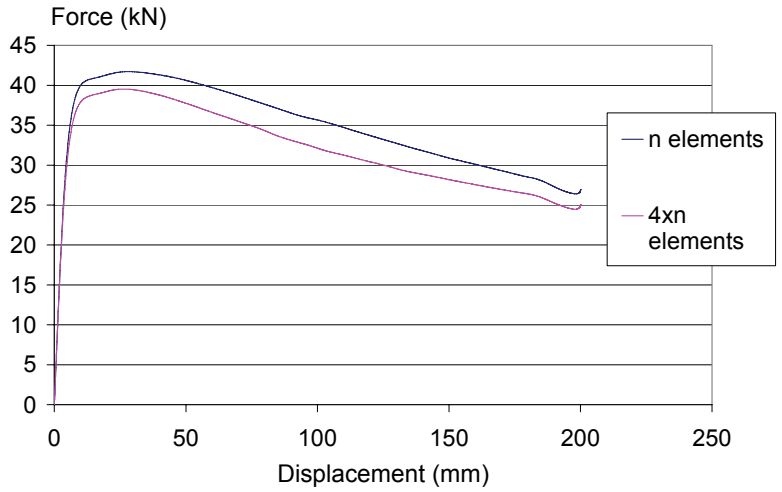

Figure 6.7. Influence of the element size. The n element curve is the uppermost.

As shown, the increase in the number of elements lowers the force response. By using smaller elements, more degrees of freedom are used. This gives a less stiff component with a larger displacement at the same load level.

6.2.2 Element Formulation

The default element formulation in LS-DYNA is the Belytschko-Lin-Tsay element (type 2). In the original cab model, however, fully integrated shell element type 16 is used. Element formulation 16 gives a more correct result. Element formulation 2 is default due to the efficiency of the elements; they save computing time with an acceptable accuracy. Figure 6.8 presents the differences in response between the two element types.

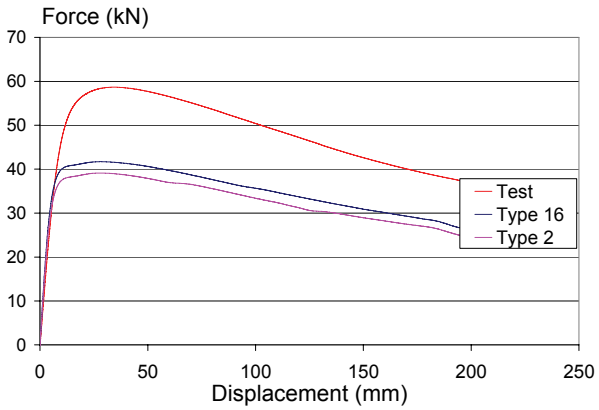

Figure 6.8. Influence of element type. The internal positions of the curves are the same as the indices

The type 16 element used in the cab model is stiffer than type 2 element since it better approximates the stress field. Type 16 is more accurate, but also more time-consuming.

6.2.3 Number of Integration Points

Shell elements are basically defined in one plane only. A thickness of each shell is defined, but there is no stress in the thickness direction. Through this plane a number of integration points are defined in which the stresses and strains are evaluated through the simulation. Basically, it is a choice between accuracy (the more integration points, the better result) and time (the more integration points, the longer the computing time). Defaults in LS-DYNA are three integration points for crash analysis, five points for metal forming and seven points for spring back analysis. Five points are however often used in this kind of simulations in order to get one point in the middle of the thickness and better accuracy due to more points than the default three.

As mentioned, five integration points are used in the cab model and therefore the first choice and also used in the reference case. Three different numbers of integration points have been used to evaluate the influence of this parameter; 2, 5 and 9 points, respectively.

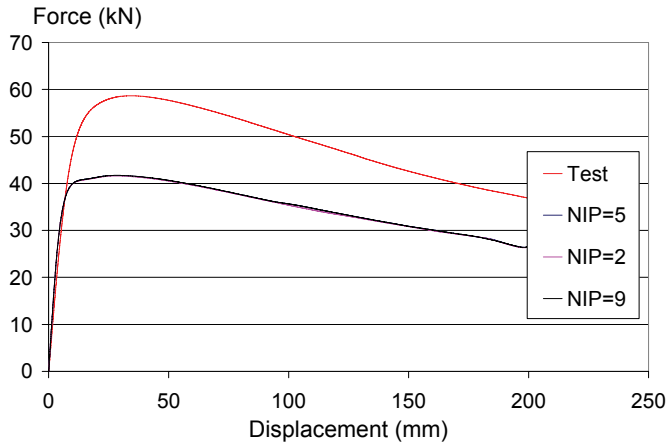

Figure 6.9. The (non-existing) influence of number of integration points (NIP)

The number of integration points does not influence the response in any significant way. The reason for this may be that the most of the structure is loaded in pure bending while the flange thickness is small compared to the width of the beams. This gives more or less constant stresses through the flange thickness.

6.2.4 Material Data

The material parameters defined in the FE model are density, Young´s modulus, Poisson's ratio and a curve defining the yield stress and relationship between true stress and true plastic strain, see Figure 6.10.

In all analyses presented in this section, Young's modulus E = 200 GPa, Poisson's ratio $\mu = 0.3$ and the density $\rho = 7800$ kg/m^3 have been used. The parameter changed and compared in this section is the curve describing the relation between true plastic strain and the yield stress.

The original cab model had a curve defining this relation for the material of the B-pillars with a yield strength of 275 MPa. An early statement in this work was that this curve probably was a bad representation of the material, which according to the supplier has a yield strength of at least 355 MPa. Therefore, the curve was scaled with a factor 1.33 which gave a yield strength of 367 MPa. The tests of the material from a beam presented in Section 5 gave a yield limit of 415 MPa. The data from testing were reformulated to be a relationship between true plastic strain and true stress as derived in Chapter 5. Since the tests were terminated when the strain was about 20 %, the curve was extrapolated with a power law function, Figure 6.10.

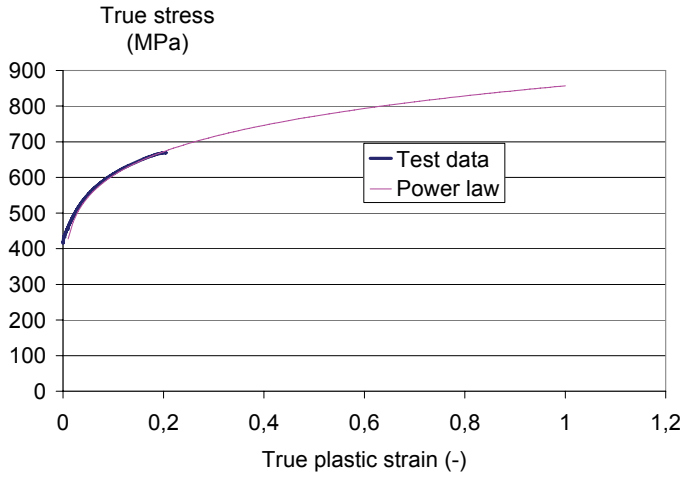

Figure 6.10. The test data in the thicker curve reaches a strain of approx. 0.2. The power law curve is used as extrapolation of the curve to the strain 1.0

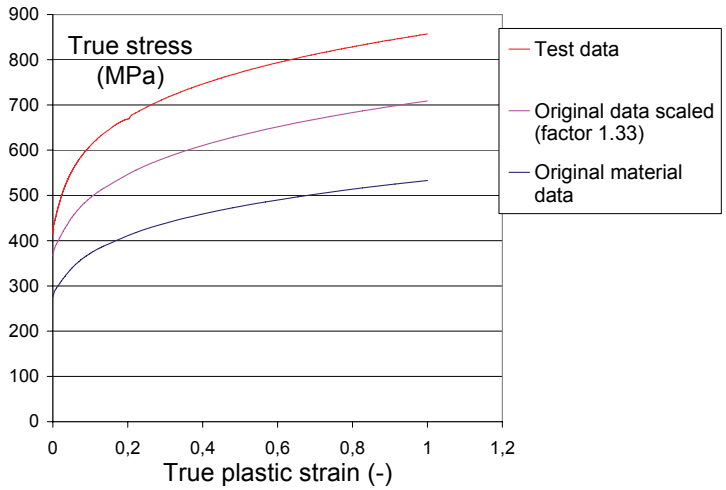

Figure 6.11. Different plastic hardening curves. The original yield strength is 275 MPa, the scaled 367 MPa and the yield strength from tests is 415 MPa. The internal positions of the curves are the same as the indices

The results from FE simulations with the three curves above used as input along with test results are presented in Figure 6.12.

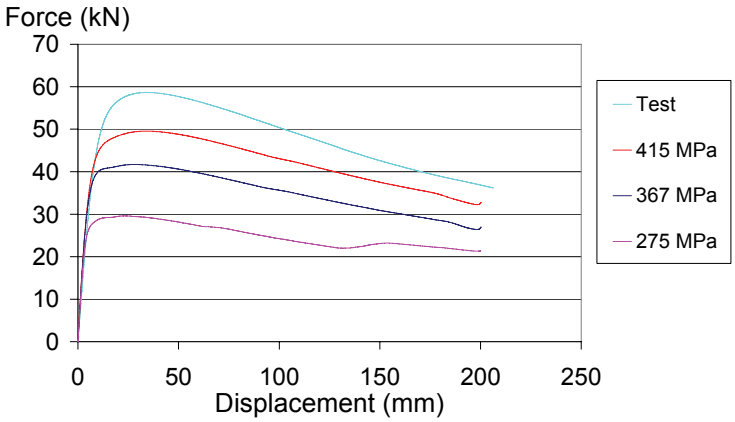

Figure 6.12. Response of different plastic hardening curves compared to test results. The internal positions of the curves are the same as the indices

Figure 6.12 presents the results from testing, simulation with nominal strength test data, simulation with the material yield strength 367 MPa and lowermost 275 MPa, respectively. The material data with yield limit 367 MPa has been used throughout the series due to the likeliness of being a correct strength before material tests were carried out. This was not, however, corresponding to the true value presented by the graph “415 MPa”, obtained from tests. These results will be further discussed later.

6.2.5 Weld Modelling

Three main methods of modelling the welds have been examined. The first is the same as in the cab model; constrained nodal rigid bodies. In this case, two or more nodes are defined as a nodal rigid body with the displacements prescribed to be the same in all included nodes. The second method of modelling the welds is using

4-noded elements and in the third method the welds are modelled using 3-noded elements. In these cases, the material modelling of the weld part is the same as for the beams. As the welds seem stiff when studying actual test structures, a case with a rigid material model applied to 4-noded shell elements has been examined as well. The three different weld-modelling methods are presented graphically in Figure 6.13 and 6.14. The results of the weld modelling aspects are presented in Figure 6.15.

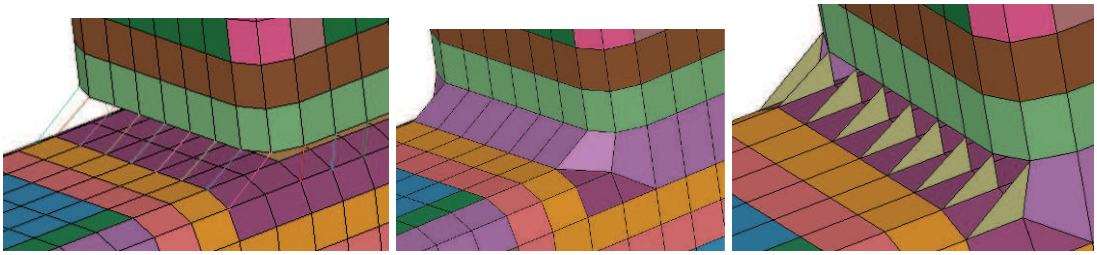

Figure 6.13. From the left: CNRB, 4-noded and 3-noded shell modelling of the weld. The 3-noded model is actually a combination of 3- and 4-noded shell elements

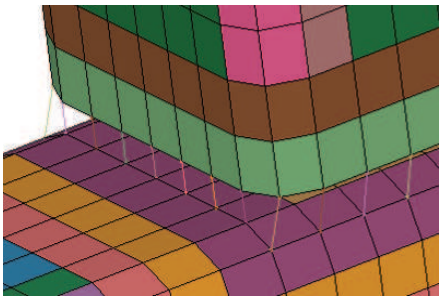

Figure 6.14. Model with short CNRB´s

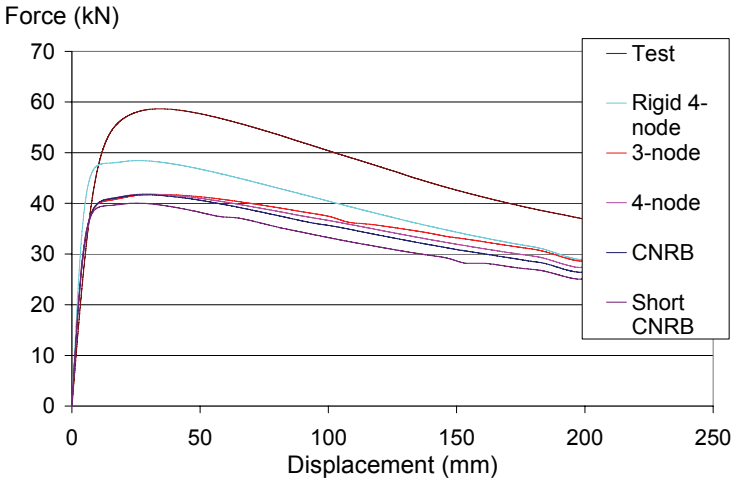

Figure 6.15. Influence of different methods of weld modeling. The internal positions of the curves are the same as the indices

From the top in Figure 6.15 the results from the test are followed by the results from a model with rigid 4-noded elements used for weld modelling. The third from the top is a model with 3-noded elements and the fourth is a model with 4-noded elements with

the same material data as the beams. The second lowermost curve is from a model with constrained nodal rigid bodies (CNRB´s) for weld modelling. In this case, the length of the CNRB´s corresponds to the length of the weld in the physical structure. The lowermost curve represents the results of where CNRB´s with the shortest possible lengths are used for weld modelling.

The results points out the importance of modelling the welds with a correct geometry. CNRB´s may be used with results reasonable accuracy as long as the length of the rigid bodies are correct.

The results from the rigid 4-noded shell element weld model may seem as the best choice. Later simulations including correct material data show however that this type of model is over-stiff.

6.2.6 Heat Affected Zone

In order to model the influence of the heat affected zones near the weld that connects the two beams, the parts may be divided into sub parts. The concept is to divide one beam into several parts in order to give different areas of the beam dissimilar material behaviour. To split up a beam, the results from the testing in Section 5.2.4 are used. Basically, three different zones are defined, as presented in Figure 6.16.

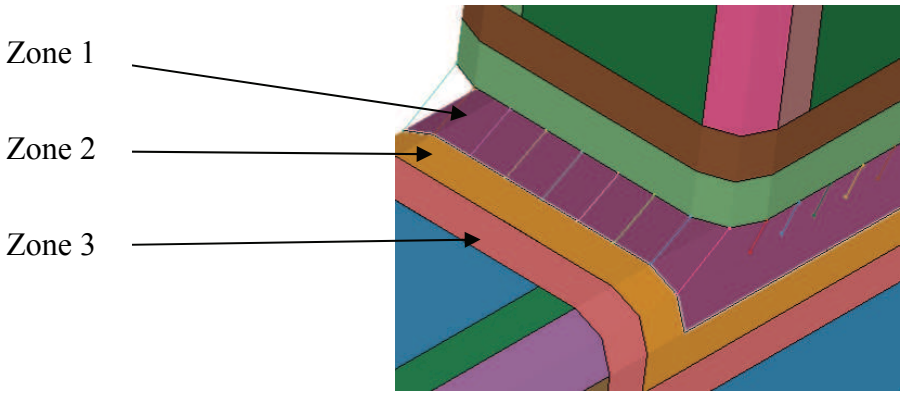

Figure 6.16 The different zones around the weld

Zone 1, in the middle of the weld, has a plastic behaviour of the material scaled with the factor 1.19. This value is obtained by dividing the Vickers hardness of the material in the weld with the nominal Vickers hardness (in this case 207/174=1.19, Chapter 5 presents the details). Zone 2 is given the factor 1.15 and zone 3 the factor 1.10. Figure 6.17 presents the meaning of this graphically and the result is presented in Figure 6.18.

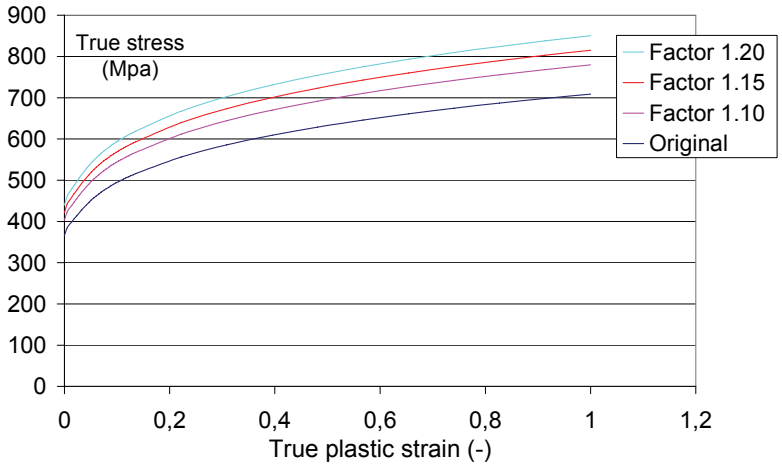

Figure 6.17. The use of scale factors due to heat affected zones. The different curves are used in the part of the beam corresponding to each hardness value

To scale the entire plastic behaviour is a generalisation made from the increased yield strength.

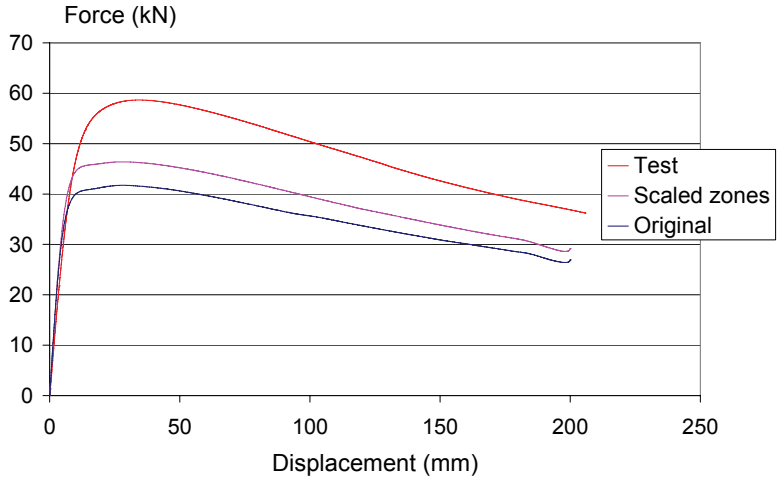

Figure 6.18. Influence of the heat affected zones. The internal positions of the curves are the same as the indices

Figure 6.18 shows the influence of the heat affected zones. Note that the basic material data still has the yield strength 367 MPa, giving the possibility to compare the original data to the case were the heat affected zones have been scaled according to hardness tests performed.

The influence from the heat affected zones is important and gives a response much stiffer than the original. A great deal of the plastic deformation is located in the heat affected areas.

6.2.7 Plastically Deformed Corners

As previously described, the corners of the beams are plastically deformed during the manufacturing process. The different hardness values due to this phenomenon are presented in Section 5.2.5 and the different zones with their scale factors for plastic behaviour are presented in Figure 6.19

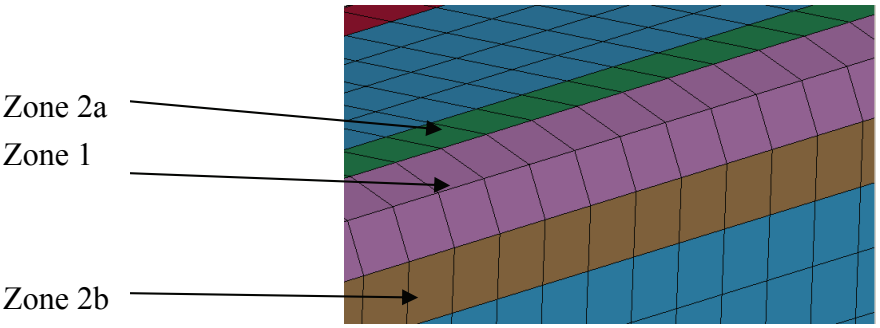

Figure 6.19. The different zones in the strain hardened corner

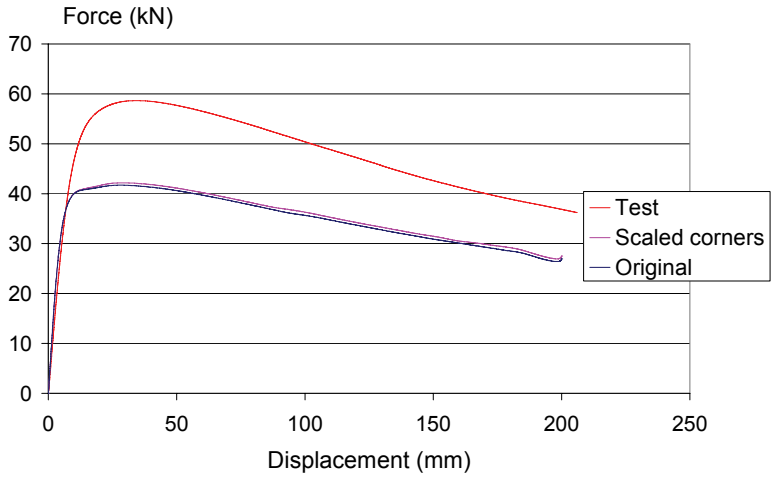

Figure 6.20. Influence of the plastically deformed corners

The influence of the strain-hardened corners is not as significant as that from the heat affected zones, probably because the corners outside the heat affected zones are not much plastically deformed.

6.2.8 Combination of Heat Affected Zones and Plastically Deformed Corners

This model is, as stated above, a combination of the modelling of heat affected zones and plastically deformed corners described in the two previous sections.

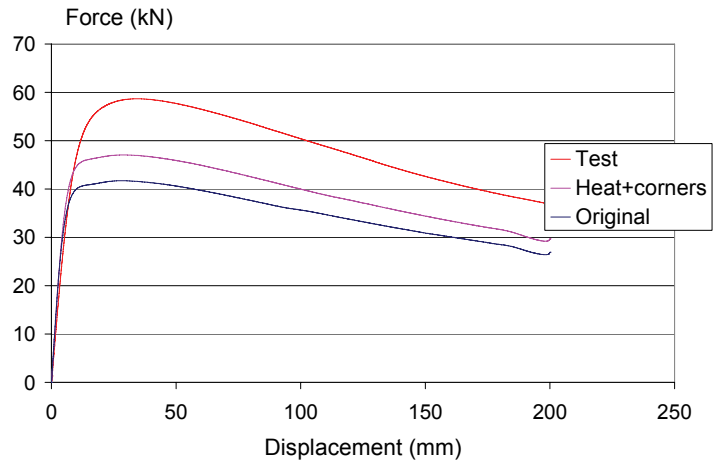

Figure 6.21. The results of modelling the heat affected zones and plastically deformed corners in the same model. The internal positions of the curves are the same as the indices

The results of heat affected zones in combination with the strain-hardened corners are not much different from that of the heat affected zones only, see previous comments.

6.2.9 Thickness Change Update

By default, no thickness updates due to membrane straining are made. That is, even if an element is heavily deformed, the thickness remains constant as defined in the input data. A simulation with thickness update due to plastic strains has been performed and the result is presented in Figure 6.22.

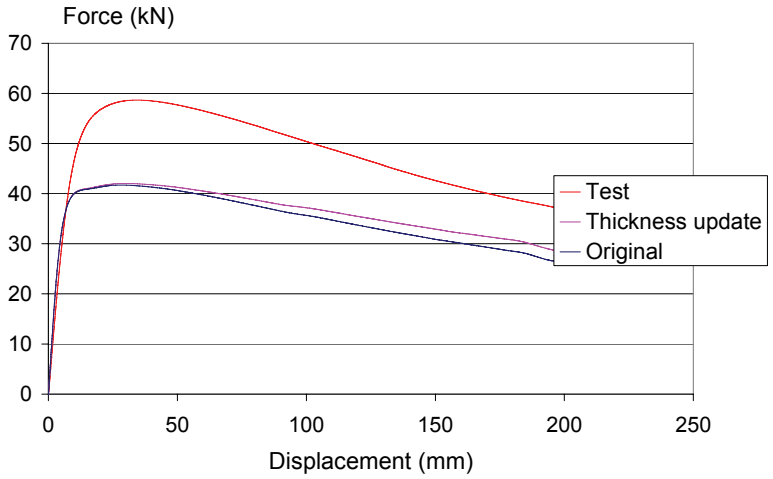

Figure 6.22. Influence of thickness update due to plastic strains

The influence of the thickness update is not significant in the area of the greatest interest, which may be defined as the left area of Figure 6.22. It is, as expected, more significant when the plastic deformations are large, to the right in the graph.

6.2.10 Globally Scaled Plastic Behaviour

The sections 6.2.6 and 6.2.7 describe the influence of the raised yield strength due to previous heating and plastic deformations of the beams. The aim of the simulation presented in this section is to present a factor to use for scaling the material curve to let the whole model share *one* material. The material data scaled are the results from tensile tests. The curve in the figure below therefore represents a combination of two models from sections 6.2.4 and 6.2.8 including a weighted, global scale factor.

If the corners influenced by plastic deformation and the areas influenced by heat near the welds are weighted relative the total amount of material, a scale factor of 1.08 is obtained. The heat affected part of the material at the joint between the welds however represents a major part of the material that plastically deforms in the simulation. Therefore, a 50 % increase of the factor 1.08 was assumed to represent the larger influence. This gives a factor of 1.12.

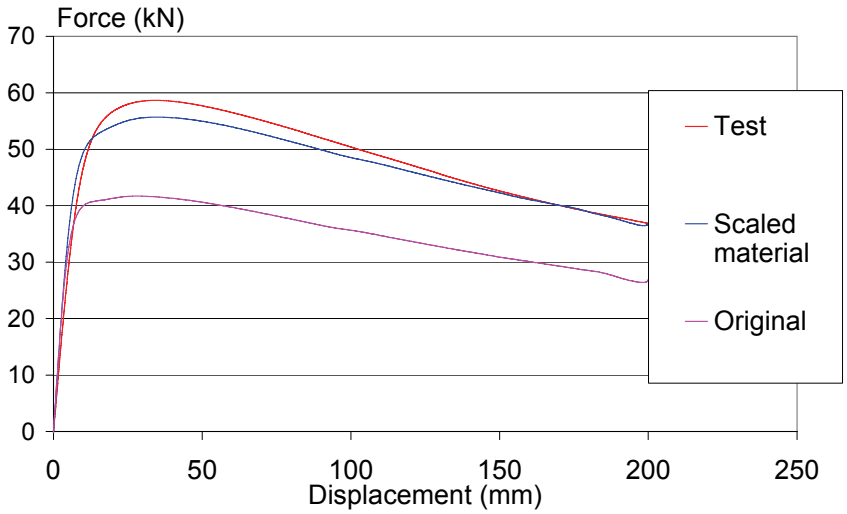

Figure 6.23. Influence of a global scale factor of 1.12 for the plastic behavior of the material. The internal positions of the curves are the same as the indices

The globally scaled material gives a response that is greatly improved. It is, however, hard to know the correct scale factor to use in different loadings and structures. The factor approximated in this case gives good results, but it is not generally applicable.

6.3 Analysis of Results and Final Combinations

A number of simulations have been carried out using different combinations of the parameters. Only the basic influences of some parameters have been presented in the previous sections.

That a decrease of element size gives a weaker response is natural. The displacements of an element are defined in the nodes which mean that a larger element gives a

reduced number of degrees of freedom. This is always a balance act between accuracy and computing time needed for an analysis.

The element formulations investigated gave slightly different results due to different approximations of the stress field. As in the case of element size, this is as well a choice between accuracy and speed; element formulation 16 is more accurate but in this case about three times more computing time consuming. The element used in all other cases, however, is element type 16 because of its performance combined with the ability to compare different results.

Regarding the number of integration points, there are no significant differences between the three cases examined - 2, 5 and 9 integration points. This could be explained by the geometric characteristics of the structure. The thickness of a beam flange is small compared to the widths which may give a behaviour that is close to constant through the flange thickness. Five integration points are used in all other cases in order to obtain comparable results.

The material data is decisively the most important factor of success in the striving for correct results. It is probably also the most extensive field of the parameters examined. The material data used in the original cab model had a yield limit of 275 MPa, and was at an early state assumed to be incorrect. This was proved to be a correct assumption later on by testing the material; the yield strength of a beam is 415 MPa and depends on the location in the beam.

No non-isotropic behaviour has been studied, which is one of the major assumptions used to describe the material. This could be justified by the loading of the structure, which gives a bending of the beams with loading in the longitudinal direction. The deformation in the buckling zone near the weld between the beams is however complex and possibly *not* negligible in the transverse direction. Despite this, the un-isotropic behaviour has not been further studied. The fact that the material data is non-homogeneous within the parts makes it even more complex to model. If corrections are made for the known diversities of plastic behaviour, good results are achievable. The attempt of scaling the whole model to a mean level with respect to yield strength succeeded with respect to obtaining results that coincides with test results from the component in this report. It is however hard to draw any general conclusions. It might not be a good factor in another loading case or structure.

The weld modelling comparisons show a large influence of the weld modelling. All models give reasonable responses for the elastic part of the compression. This is not enough; a correct behaviour is demanded in the plastic regime as well. The comparisons made show that a model with rigid shell elements gives a too large stiffness of the structure. When comparing the other cases, the most important factor seems to be to model the weld with a *length corresponding to the reality*. That is, the size (length) of the weld model should be the same as the actual weld. If this is done and combined with correct material data, the maximum load will be correct, see Figure 6.24.

In order to describe the plastic behaviour throughout the simulation correctly, the 3-noded shell element representation gives satisfying results. This model is the one with the most realistic representation of the weld material.

No statistical studies have been performed, which makes the combination of different combinations of parameters somewhat hazardous. Errors may still be included in the result but cancelled out by each other. The most correct modelling aspects however ought to be a combination of small elements, material data from tensile tests and hardness tests combined with 3-noded shell elements for the weld modelling and element formulation 16. The results of this combination prove the validity of the investigation performed, Figure 6.24.

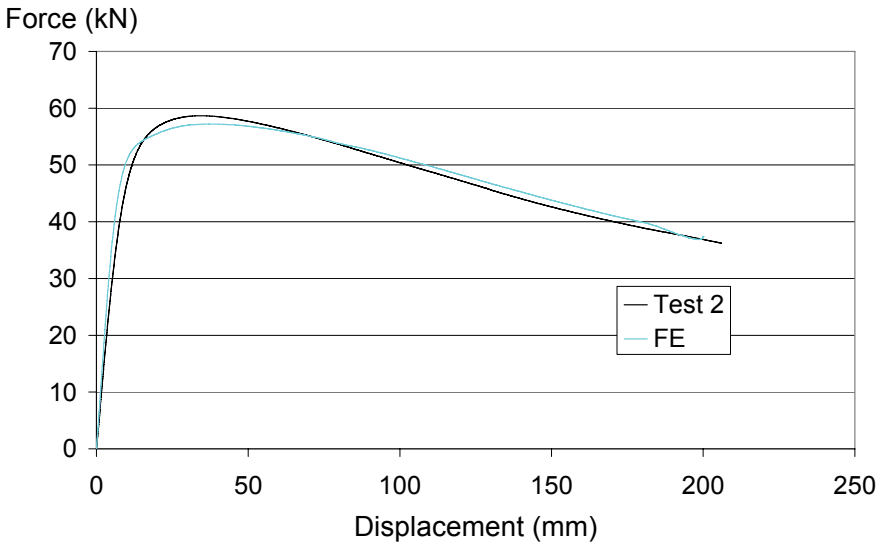

Figure 6.24. The most correct combinations of parameters give good results. The most important parameters in this context are material data according to yield- and hardness tests and 3-noded shell elements with a size corresponding to reality

The results above are satisfying with respect to correctness. Despite this, the parameters used are not that good in means of implementation in a cab model. That would be very time-consuming due to a great deal of manual work as well as a computing time needed for the analysis in the order of eight times longer than the original.

The combination of factors to use in the cab model is not utterly obvious, but a suggestion of modelling aspects are to use the original size of elements combined with somewhat scaled yield test data; for example a factor of 1.10 might be used. The lowered factor 1.10 instead of the previously used 1.12 is suggested because of the deformation modes. In the tested component a great part of plastic deformations are found in the heat affected zone. In the cab, deformations are more spread along the beams and the beams are generally longer than the one used in the component.

Further, it is important to study the welds of the cab with respect to geometry – constrained nodal rigid bodies may be used as long as the lengths of the welds are represented properly.

The combination suggested above gives component model results according to Figure 6.25.

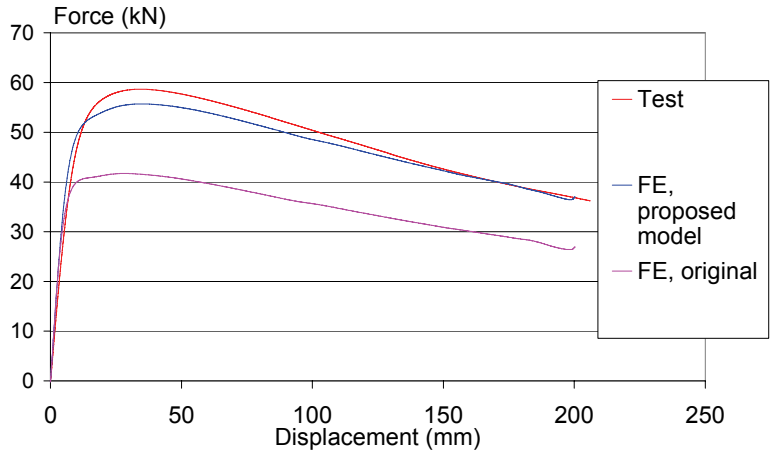

Figure 6.25. Results obtained with the proposed setup of parameters compared to test results and the original FE results. The internal positions of the curves are the same as the indices

The proposed set of parameters is based on globally scaled material properties with the factor 1.10 and CNRB´s with lengths corresponding to the length of the physical weld. It gives reasonable accuracy without extending the computational work too much.

7 Modified Simulations of ROPS Test Performed by ERAB

Three main changes have been done in the cab model. These are change of material properties, changes in geometry/weld modelling and the implementation of a sequential loading, respectively. The different changes and their influence on the results are presented in this section. All results presented are from longitudinal loading which had the largest errors in the original simulation. All simulations of the cab model have been performed by ERAB.

7.1 Material Data

In the original model, the used nominal material data were not at all correct according to later performed tests. With an updated model using material data with a yield strength of about 440 MPa, corresponding approximately to the recommendations in Section 6, the results are improved, Figure 7.1.

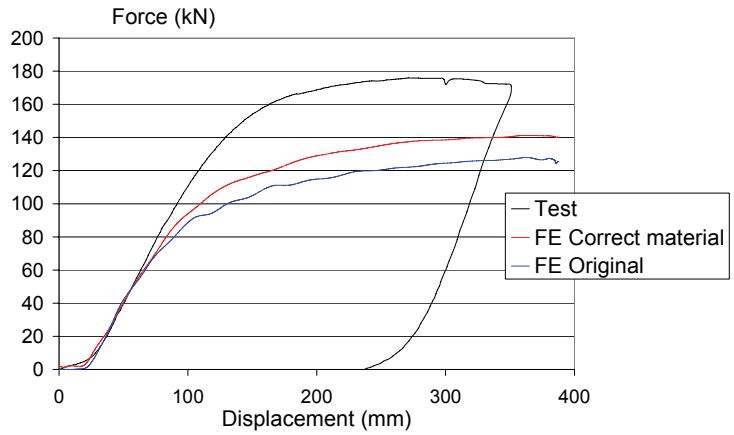

Figure 7.1. The influence by using correct material data.
Longitudinal loading. The internal positions of the curves are the same as the indices

By using the correct material data, results are improved. They are however still far from satisfying; more errors are present in the model.

7.2 Material Data and Weld Modelling

In this model, in addition to the material data there are further corrections made to the model. Some of the welds have been improved and other corrections of geometry and modelling have been made.

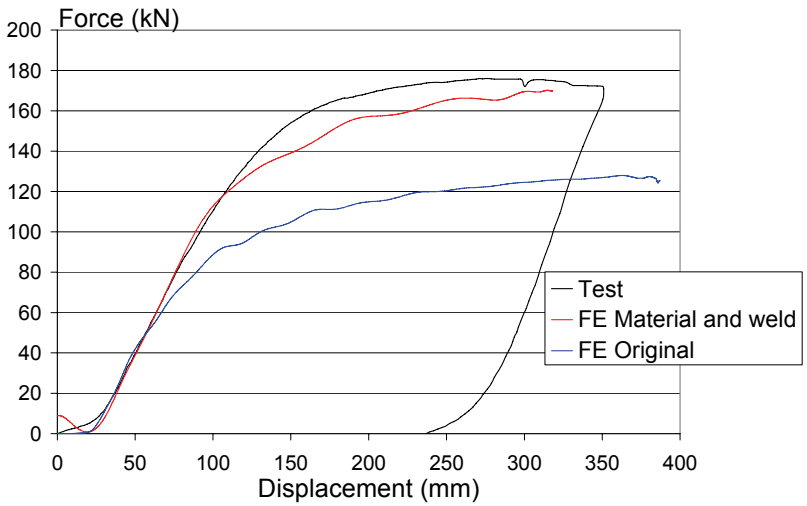

Figure 7.2. The influence of correct material data combined with updated weld modeling and minor geometric changes. Longitudinal loading. The internal positions of the curves are the same as the indices

By use of correct material data and updating the weld modelling the results tend to converge towards the test results. There are however still one major simulation aspect to alter.

7.3 Material Data, Weld Modelling and Sequential Loading

The test is carried out in a sequence of three loadings – lateral, vertical and longitudinal. The original simulation did only cover the last part, the longitudinal loading. By excluding the influence of the former lateral and vertical loadings, important geometry – and material aspects are left out. The results obtained from a simulation including the full loading sequence, using the updated material data and weld/geometry changes, are presented in Figure 7.3.

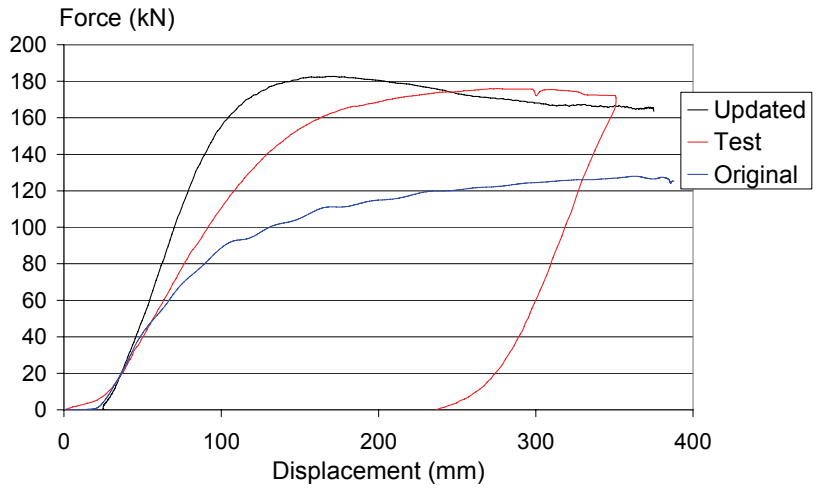

Figure 7.3. Results from a simulation whose model is updated with respect to material data, weld modelling and sequential loading. The internal positions of the curves are the same as the indices

The results are somewhat over-stiff. The reasons for this are not obvious; material modelling may be part of the answer. The material model used is isotropic and includes strain hardening from tensile tests. This might over-estimate the strength of the material in the perpendicular directions of the tested. Another source of errors may be the thick plate that the cab is mounted at. This plate is significantly deformed in the test as well as in the simulation. The difference is small and hard to make corrections for. In the lateral loading, the plate is bent while the vertical loading presses the plate back, see Figure 7.4. Small differences in how far the vertical loading is taken gives differences in how bent the plate will be prior to the longitudinal loading. If the plate is just a little more bent in the simulation than in the test, this might give an over-stiff structure.

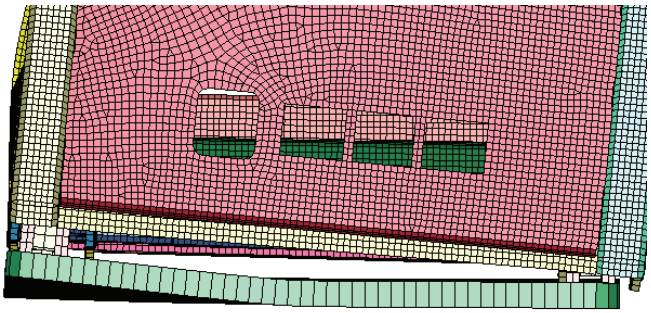

Figure 7.4. The bottom plate is heavily deformed by the lateral loading. (Parts of no interest for this information has been excluded)

Figure 7.4 presents the matter clearly; the lateral loading has been performed from left to right in the figure. By the vertical loading, the plate will be pressed down before the longitudinal loading takes place, in direction into the figure.

The plate discussed is 40 mm thick. It is still represented by shell elements, which could be a too rough estimation of the behaviour. A representation with solid elements, using a number of rows of elements through thickness, might give better results due to the more degrees of freedoms applicable in the plate.

8 Results

The objective of this thesis was to find the reasons of divergence between test and simulation results from the ROPS test on a cab structure. A second objective was to exclude as many parameters as possible from the potential reasons of divergence. The parameters that are *not* reasons of divergence are not presented in this section, for those the reader is referred to previous chapters.

One main result is the various material characteristics in a welded structure. The real properties of a beam differ distinguishably from nominal data provided by the material supplier and differ depending on the location in the beam. This is certainly due to at least two factors, probably three. Firstly, the corners of a beam are strain hardened while forming a metal sheet into a beam. Secondly, the beams are strengthened with respect to yield strength by the weld that joins each beam along an entire side. The third factor is that the material is originally stronger than the nominal data provided by the material supplier. Further, joining beams with welds affects the material surrounding the welds due to the heat. Due to this effect, the material is strengthened even further.

Another major result is the influence of weld modelling; it is important to model the welds with respect to their real size. In the case of large plastic deformations, the choice of model affects the results to some extent. The best way examined is to use 3-noded shell elements that distributes the material of the weld in the most realistic way.

By updating the cab model with the results presented above, major improvements are obtained on the ROPS-simulation results. By carrying out the whole sequence of loading instead of the longitudinal only, the response obtained is somewhat over-stiff. The reasons of this will be further investigated by ERAB and is not included in this thesis.

The outcome results is however far better than the original simulation results. Due to corrections of material data, weld modelling and some geometric modelling errors in the model, the simulation results have been improved significantly.

9 Conclusions

There are many parameters and aspects involved in a cab model for simulation of the ROPS-test. The most important aspects according to this thesis are presented in this section.

Correct material data is an absolute requirement to get acceptable results. In this case, it involves quite complex and time-consuming modelling which is hard to avoid. A simplification of the material properties by globally scaling of the plastic behaviour has been examined but needs further verification before being used more generally. This way of simplifying the problem is hard to use due to the fact that different loading cases give plastic behaviour in diverse areas.

Weld modelling is another time-consuming task. The method proposed in this thesis is very time-consuming because of its large amount of manual work. It does, however, seem to give satisfying results. In an elastic simulation the problems would not be present. The previously used method of weld modelling gives reasonable results if changed slightly to be used in a more representative way. That is, it is important to model the welds in a way that gives geometric agreement with the physical welds.

10 Possible Future Work

The next focus of the task is to examine the influence of how far the lateral loading is taken as discussed in Section 6. This will be continued at ERAB and is not included in this thesis.

A number of different parameters have been examined with respect to influence on the response. No statistical treatment of the data has been performed. This might be done including for example a sensitivity analysis which could give more detailed information about the influence of different parameters.

The assumption of linearity between Vickers hardness and yield strength is only partially verified. Even though one set of tests has been carried out to verify the linearity claimed by Davis et al. (1998) and Peng et al. (2005), there are still some uncertainties on this matter. The verification deals with the longitudinal weld in a beam – the linear relation regarding the corners and the weld joining two beams have not been verified.

References

Dahlberg, T. (2001) T*eknisk hållfasthetslära*, Studentlitteratur, Lund

Davis, J. R. et al. (1998) *Metals Handbook, Second Desk Edition,* ASM International, Chagrin Falls

Hallquist J. O. (2006) *LS-Dyna Theory Manual,* Livermore Software Technology Corporation, Livermore

ISO 3471-1.2 (2005) *Earth-moving machinery – Rollover protective structures; laboratory tests and performance requirements – Part 1: Metallic structure*
(Note: this is a draft for the next standard and is *not* an established ISO Standard).

LS-DYNA (2005) *Keyword user's manual* Version 971 Beta Version, Livermore Software Technology Corporation, Livermore

Odenö H., Klarbring, A. (1984) *Plasticitetsteori,* LiTH–IKP–S–257, Division of Solid Mechanics, Linköping University, Linköping

Peng Ru et al. (2005) *Experimental Evaluation of Fatigue and Fracture*, Division of Engineering Materials, University of Linköping, Linköping

SS-EN 10002-1 (2001) *Metallic materials – Tensile testing Part 1: Method of test at ambient temperature*, 2nd Edition, Swedish Standards Institute, Stockholm

XYZ Scientific Applications, Inc. (2001) *TrueGrid ManualVersion 2.1.0,* Livermore

Appendix A: Drawings of Component

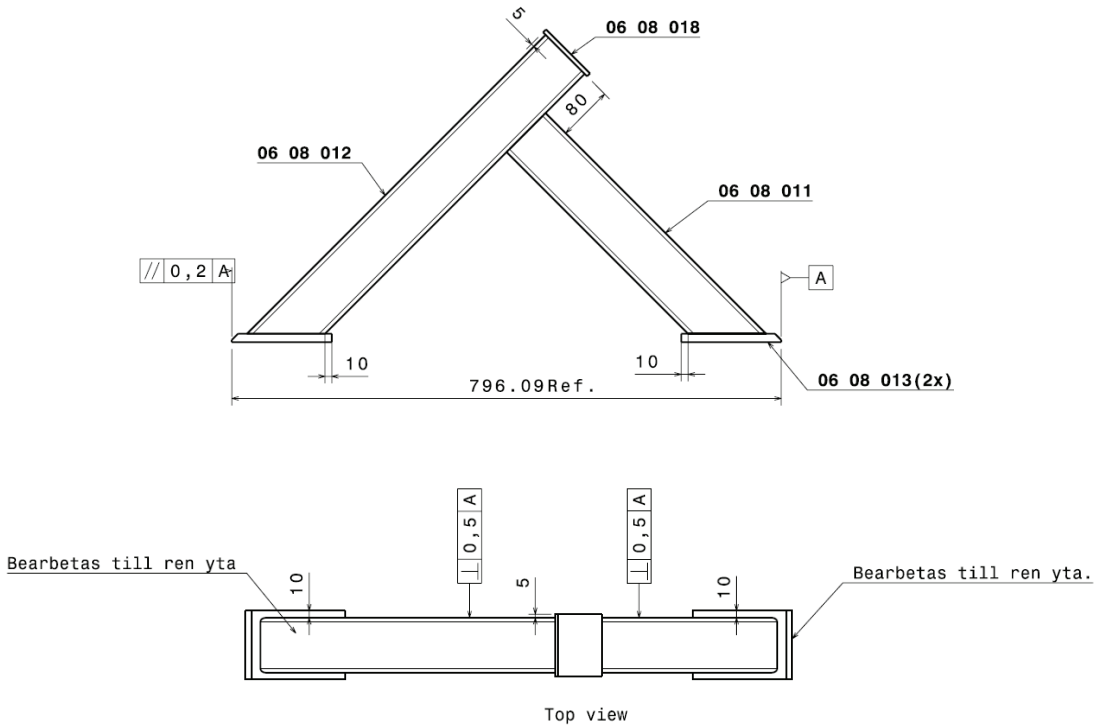

Figure A1. Assembly drawing

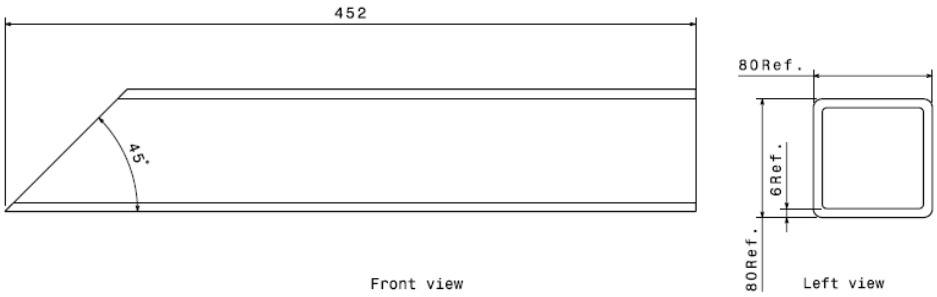

Figure A2. Short beam, part 06 08 011

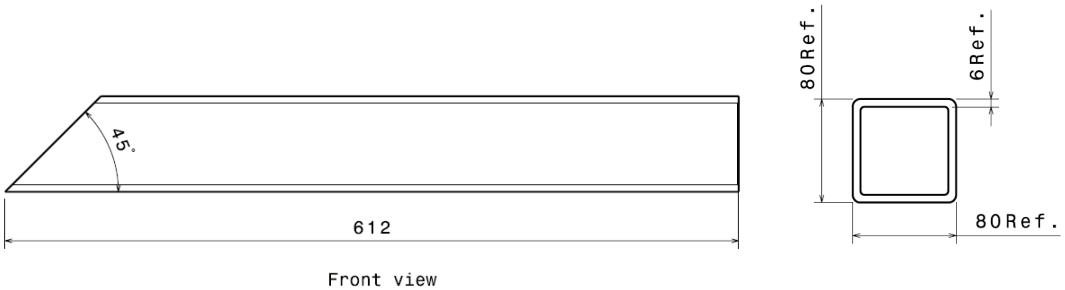

Figure A3. Long beam, part 06 08 012

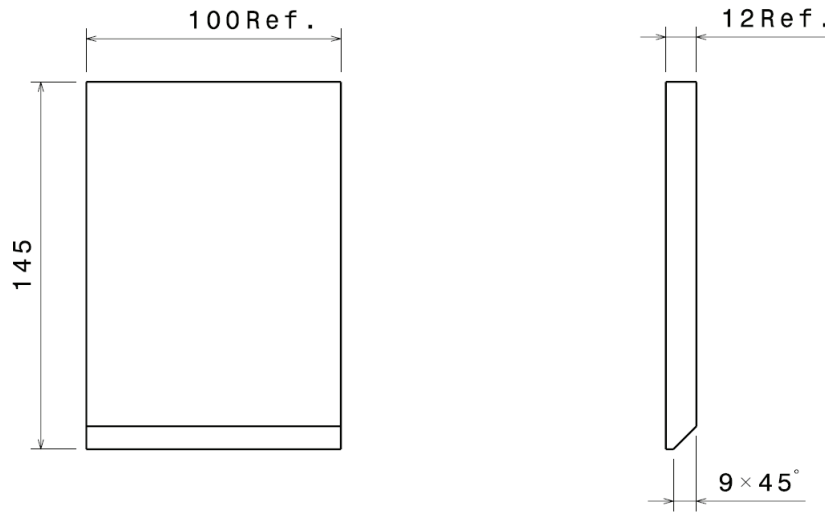

Figure A4. Force plate, part 06 08 013

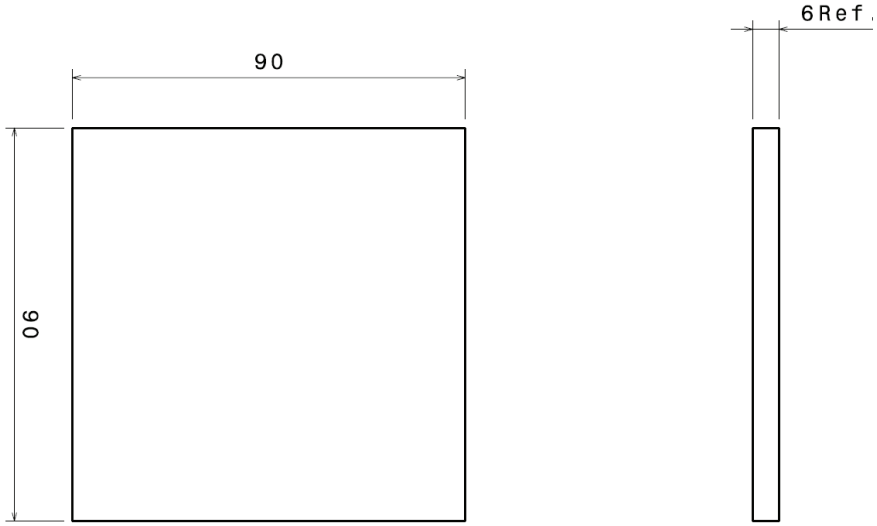

Figure A5 End plate, part 06 08 018